Investigating microclimate effects in an oasis-desert interaction zone

Liu, Rui; Sogachev, Andrey; Yang, Xiaofan; Liu, Shaomin; Xu, Tongren; Zhang, Junjie

Published in:
Agricultural and Forest Meteorology

Link to article, DOI:
10.1016/j.agrformet.2020.107992

Publication date:
2020

Document Version
Publisher's PDF, also known as Version of record

Agricultural and Forest Meteorology 290 (2020) 107992

Contents lists available at ScienceDirect

Agricultural and Forest Meteorology

journal homepage: www.elsevier.com/locate/agrformet

Investigating microclimate effects in an oasis-desert interaction zone

Rui Liu[a,b], Andrey Sogachev[c], Xiaofan Yang[a], Shaomin Liu[a,*], Tongren Xu[a], Junjie Zhang[a]

[a] State Key Laboratory of Earth Surface Processes and Resource Ecology, Faculty of Geographical Science, Beijing Normal University, Beijing 100875, China
[b] Institute of Urban Study, School of Environmental and Geographical Sciences (SEGS), Shanghai Normal University, Shanghai 200234, China
[c] Wind Energy Department, Technical University of Denmark, Risø Campus, Roskilde 4000, Denmark

ARTICLE INFO

Keywords:
Oasis-desert interactions
Computational fluid dynamics
Microclimate effects
Oasis sustainability

ABSTRACT

To investigate oasis-desert microclimate effects, we performed a series of numerical simulations in an idealized oasis-desert system based on an improved computational fluid dynamics (CFD) model for simulating atmospheric boundary layer flows, air temperature and humidity. Numerical simulations were designed based on the hydrometeorological observations obtained during the HiWATER-MUSOEXE (Heihe Watershed Allied Telemetry Experimental Research, Multi-Scale Observation Experiment on Evapotranspiration over heterogeneous land surfaces) campaign. The results are summarized as follows: (1) Oasis-desert interactions are significantly affected by background wind conditions. We observed the oasis-desert local circulation under calm background wind conditions and the oasis thermal internal boundary layer under low wind speed conditions induced by hydrothermal contracts. These interactions will disappear when the background wind speed is sufficiently high, and there is only an oasis dynamic internal boundary layer caused by the aerodynamic roughness length contrast. (2) Oasis-desert interactions lead to a series of microclimate effects, including the oasis cold-wet island effect, air humidity inversion effect within the surrounding desert and oasis wind shield effect, which are important for the stability and sustainability of the oases-desert ecosystem. (3) The hydrothermal conditions due to the difference between the oasis and desert, the vegetation fraction and distribution patterns impact the oasis-desert microclimate effects. The intensity of oasis-desert interactions increases with the land surface temperature (LST) difference in the oasis-desert. The oasis-desert interactions are gradually strengthened with the increase of the vegetation fraction within the oasis. Integrated ecological and economic benefits of the oasis, the oasis vegetation pattern, which includes the croplands and shelterbelts staggered within the oasis and the shelterbelts surrounding the outside, is beneficial to limiting the loss of water vapor and preventing sandstorms from the oasis. The findings of the current study improve the fundamental understanding of the microclimate and provide implications for maintaining the sustainability of oasis-desert ecosystems.

1. Introduction

Arid and semi-arid regions constitute approximately 25% of the world's total land surface (Harrison and Pearce, 2000; Scanlon et al., 2006), wherein deserts and oases generally act as landscape matrices and mosaics (Cheng et al., 2014). The oases are the basis of human life and economic development, supporting more than 95% of the population in the arid regions of China with less than 5% of the total area of arid regions (Chu et al., 2005; Li et al., 2016). Freshwater supplied from an inland river basin sustains the oasis and prevents it from desertification (Xue et al., 2018). Since the last century, many inland river basins have suffered from a series of environmental issues, such as dryness of rivers and lakes, degradation of natural vegetation, land desertification, and sandstorms (Crétaux et al., 2009; Stanev et al., 2004; Zhao et al., 2013; Stone, 2015). Therefore, supporting oasis sustainability and providing stable maintenance and development of oasis ecosystems is a crucial task (De Azagra et al., 2004; Li et al., 2016).

The oases and surrounding deserts are independent yet contradictive and interactive. Heat, water vapor and momentum exchanges occur between the two individual systems due to the different land surface hydrothermal conditions (such as land surface temperature (LST)), soil moisture and aerodynamic roughness length), which stimulate oasis-desert interactions (Li et al., 2016). The transfer of heat from the desert to the oasis is beneficial to the productivity and evapotranspiration of vegetation. Simultaneously, the transfer of water vapor from the oasis to the near-surface layer of the surrounding desert positively affects the maintenance of desert vegetation (Meng et al.,

* Corresponding author.
E-mail address: smliu@bnu.edu.cn (S. Liu).

https://doi.org/10.1016/j.agrformet.2020.107992
Received 2 December 2019; Received in revised form 28 March 2020; Accepted 2 April 2020

2012). The oasis-desert interactions, including the oasis-desert local circulation and airflows within the oasis inner boundary layer, lead to a series of oasis-desert microclimate effects, i.e., oasis wind shield effect, oasis cold-wet island effect (oasis effect) and air humidity inversion effect in the surrounding desert (desert effect) (Wen et al., 2014). The oasis-desert microclimate effects are characterized by decreased wind speed (Zhao et al., 2008; Chen et al., 2015; Zhang et al., 2017; Liu et al., 2018a), thermal inversion and negative sensible heat flux over oases during the growing season (Bavel, 1967; Oke and Cleugh, 1987; Su and Hu, 1988; Liu et al., 2011; Hao et al., 2016; Xu et al., 2017), increased atmospheric and soil moisture (Saaroni et al., 2004; Hao et al., 2016), air humidity inversion and negative (downward) water vapor flux near the surface layer over the surrounding desert during the daytime, and vice versa at night (Zhang and Huang, 2004; Chen et al., 2015). Therefore, these microclimate effects not only cool the oasis surface but also create a net flux of moisture from the oasis into the surrounding desert, which is essential to maintain climate conditions of arid and semi-arid regions and the sustainable development of oases-desert ecosystems (Li et al., 2016).

According to Meng et al. (2012), the main factors that affect the microclimate effects are the oasis size, background wind speed, vegetation fraction of the oasis, and the difference in the hydrothermal conditions between the oasis and desert. Extensive studies have investigated oasis-desert interactions based on field observations (Taha et al., 1991; Saaroni et al., 2004; Potchter et al., 2008; Xu et al., 2017; Xue et al., 2018) but are limited in the mechanism understanding of the oasis microclimate effects (Hao et al., 2016). Numerous mesoscale numerical simulations provide useful mechanistic explanations (Liu et al., 2004; Chu et al., 2005; Meng et al., 2009, 2015; Georgescu et al., 2011; Zhang et al., 2017). However, the grid resolution of mesoscale models is usually at the kilometer scale, ignoring the fact that the momentum (induced by crops, orchards, shelterbelts and residential areas) and the spatial heterogeneity of surface hydrothermal conditions (induced by irrigation) in the oasis interior are at the meter scale. As Macqueen et al. (1995) and Fernando et al. (2019) indicated, improving only the grid resolution of mesoscale models may increase simulation errors. Thus, the computational fluid dynamics (CFD) method, with its powerful and flexible simulation capabilities, should be more suitable for studying high spatial (~m) and temporal resolution (~s) atmosphere boundary layers over heterogeneous landscapes (Foken et al., 2011; Lee et al., 2015). Wang and Li (2016) used commercial CFD software to study urban heat island circulation but without considering the effect of vegetation. Sogachev et al. (2002) developed a CFD model named SCADIS (SCAlar DIStribution) to investigate the physical processes within both the plant canopy and the planetary boundary layer (PBL). These studies demonstrate that CFD can be a powerful tool to understand local circulation better and quantify the impacts of vegetation parameters on the microclimate. However, there is no rigorous CFD studies have been performed on the oasis-desert interactions, especially on the microclimate effects, and the effect of vegetation on turbulent flow or heat and water vapor fluxes has mostly been neglected in CFD simulations. Thus, in the current study, we aim to develop a CFD model that can accurately prescribe the radiation distribution mechanics and energy balance over heterogeneous land surfaces to study the microclimate effects in the oasis-desert interaction zone.

In this study, an improved CFD model was developed based on the OpenFOAM platform (https://www.openfoam.com/) to capture the transfer of heat, water vapor and momentum between the land surface with vegetation and the atmospheric boundary layer, which considers radiation distributions within vegetation and the energy balance of vegetation and soil. Then, the CFD model was utilized to simulate the atmospheric boundary layer flows, air temperature and humidity over an idealized oasis-desert system where the parameters of the vegetation, soil and initial boundary conditions were configured based on real observations. Moreover, the oasis-desert interactions were further analyzed, and the impacts of weather conditions, the hydrothermal conditions due to the difference between the oasis and desert on the microclimate processes were investigated. Finally, we explored and discussed the pathways for oasis maintenance.

2. CFD model descriptions

2.1. CFD model improvements and implementations

In order to simulate the interactions between the vegetation and atmospheric boundary layers, we improved a previously-developed CFD model by incorporating boundary and surface layer turbulence and surface layer vegetative processes and implemented it into an open source, massively-parallel CFD solver OpenFOAM. The commonly-adopted CFD model calculates the flow and temperature fields following the mass, momentum and energy conservation laws in an iterative way. In the current study, the original Reynolds Averaged Navier-Stokes (RANS) equations and the standard k - ε turbulence equations serve as the major components of the governing equations. In addition, a serious of modules taking account of radiation, leaf energy balance and soil energy balance were customized to describe the energy and water vapor transfer that occur inside the vegetation. Also, we added specific source terms to the governing equations that consider the effects of vegetation and buoyancy force. Numerically, the vegetation canopy is divided into several layers. The leaf area density (*LAD*) that characterize the effects of vegetation on the meteorological regime is applied to each grid of the CFD mesh. All the modules and source terms were programmed in C++ and implemented into OpenFOAM.

Details of the in-house developed modules are given in the following sections. The radiation module is used for calculating the net radiative flux of the vegetation canopy and soil (Section 2.4.1). The leaf energy balance module is used for obtaining the leaf surface temperature and humidity (Section 2.4.2). The soil energy balance module is used as the bottom boundary condition of the temperature (Section 2.4.3). Wind speed, temperature and humidity of the ambient air were calculated using the governing equations of mass, momentum and energy with source terms (Sections 2.2 and 2.3). All the modules were run iteratively untilconvergence using the criterion that the dimensionless residual errors were $\leq 10^{-5}$ for each variable (Fig. 1).

2.2. Governing equations and turbulence model

The airflow fields are solved using the incompressible RANS equations (Anderson and Wendt, 1995). The impacts of vegetation are represented as additional source terms of the governing equations. Under the Boussinesq approximation, the equations for conservation of momentum, heat and water vapor exchange between the land surface with vegetation and atmosphere boundary layer can be written as follows (Manickathan et al., 2018):

$$\frac{\partial \overline{u_i}}{\partial t} + \overline{u_j}\cdot\frac{\partial \overline{u_i}}{\partial x_j} = -\frac{1}{\rho_k}\frac{\partial \overline{p}}{\partial x_i} + \frac{\partial}{\partial x_j}\left\{(\nu+\nu_t)\left[\left(\frac{\partial \overline{u_i}}{\partial x_j}+\frac{\partial \overline{u_j}}{\partial x_i}\right) - \frac{2}{3}\left(\frac{\partial \overline{u_k}}{\partial x_k}\right)\delta_{ij}\right]\right\} + g_i[1-\beta(\overline{T}-\overline{T_0})] + S_u \quad (1)$$

$$\frac{\partial \overline{T}}{\partial t} + \overline{u_j}\cdot\frac{\partial \overline{T}}{\partial x_j} = \frac{\partial}{\partial x_1}\left[\left(\frac{\nu}{Pr}+\frac{\nu_t}{\mathrm{Pr}_t}\right)\frac{\partial \overline{T}}{\partial x_1}\right] + \frac{\partial}{\partial x_2}\left[\left(\frac{\nu}{Pr}+\frac{\nu_t}{\mathrm{Pr}_t}\right)\frac{\partial \overline{T}}{\partial x_2}\right] + \frac{\partial}{\partial x_3}\left[\left(\frac{\nu}{Pr}+\frac{\nu_t}{\mathrm{Pr}_t}\right)\left(\frac{\partial \overline{T}}{\partial x_3}+\gamma_a\right)\right] + S_T \quad (2)$$

$$\frac{\partial \overline{q}}{\partial t} + \overline{u_j}\cdot\frac{\partial \overline{q}}{\partial x_j} = \frac{\partial}{\partial x_j}\left[\left(\frac{\nu}{Sc}+\frac{\nu_t}{Sc_t}\right)\frac{\partial \overline{q}}{\partial x_j}\right] + S_q \quad (3)$$

where x_i (i = 1, 2, 3, $x_1 = x$, $x_2 = y$, $x_3 = z$) represent the longitudinal, lateral and vertical directions, respectively; t is time (sec); $\overline{u_i}$ is the mean velocity component along x_i direction (m/s); $\overline{T}$ is the mean air

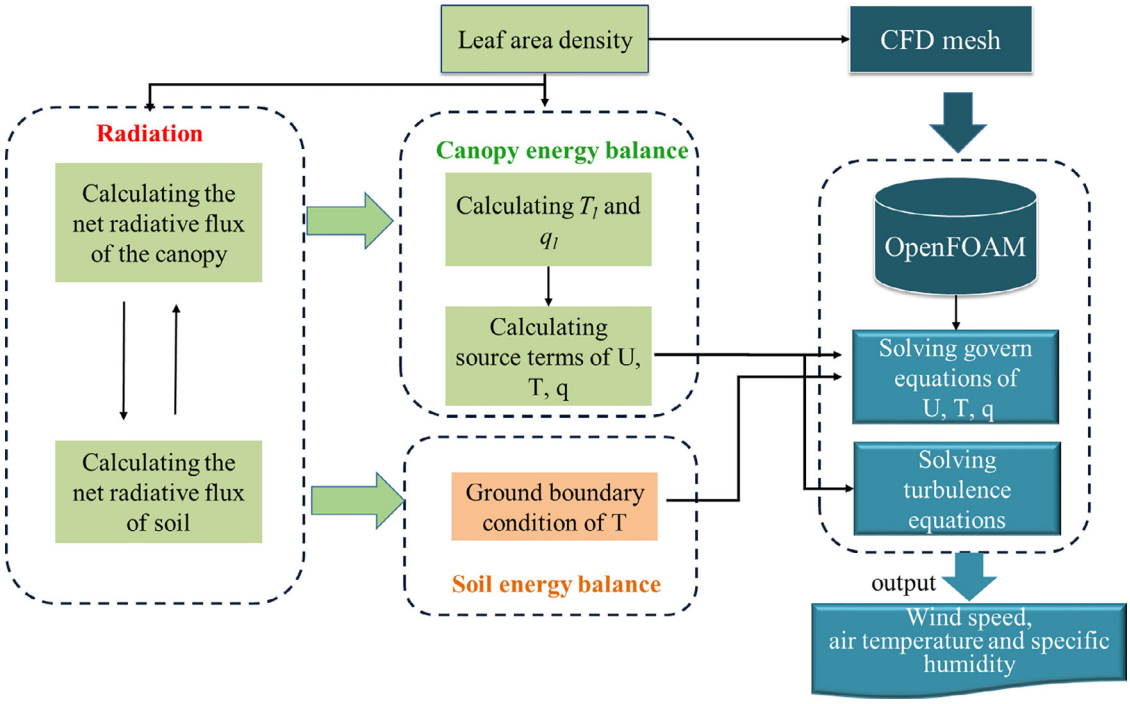

Fig. 1.. Flowchart of the CFD solver.

temperature (K); $\overline{T_0}$ is the reference temperature (K); q is the air specific humidity (g/kg); p is the static pressure (Pa); g_i is the gravitational acceleration, which is (0,0, −9.81) m/s^2. The buoyancy force is considered using the Boussinesq approximation for air density variations. The air density is calculated by $\rho = \rho_k \times \rho_0$, where ρ_0 is the air density at the reference temperature, which is taken as 1.225 kg/m^3. The effective kinematic density ρ_k is calculated as a linear function of temperature (dimensionless) (Pieterse and Harms, 2013):

$$\rho_k = 1 - \beta(\overline{T} - \overline{T_0}) \tag{4}$$

where the thermal expansion coefficient β is defined as $-(\frac{1}{\rho_0})\frac{\partial\rho}{\partial\overline{T}}$ (K^{-1}). *Pr, Sc, Pr$_t$* and *Sc$_t$* are the Prandtl number, Schmidt number, turbulent Prandtl number, and turbulent Schmidt number, which are taken as 0.9, 0.9, 0.7 and 0.7, respectively (Tominaga and Stathopoulos, 2007). ν is the molecular viscosity, which is taken as 1.45×10^{-5} m^2/s; γ_a is the dry adiabatic lapse rate, which is 0.0098 K/m.

The standard k - ε turbulence model (Launder and Spalding, 1974) is used to estimate the turbulent viscosity $\nu_t = C_\mu\frac{k^2}{\varepsilon}$, in which two prognostic equations are solved for the turbulent kinetic energy (k) and its dissipation rate (ε). The method of Sogachev et al. (2012) is used to account for the buoyancy and vegetation drag effect in the equations.

$$\frac{\partial k}{\partial t} + \overline{u_j}\cdot\frac{\partial k}{\partial x_j} = \frac{\partial}{\partial x_j}\left[\left(\nu + \frac{\nu_t}{\sigma_k}\right)\frac{\partial k}{\partial x_j}\right] + \nu_t\left(\frac{\partial\overline{u_i}}{\partial x_j} + \frac{\partial\overline{u_j}}{\partial x_i}\right) - \varepsilon + G_b + S_k \tag{5}$$

$$\frac{\partial \varepsilon}{\partial t} + \overline{u_j}\cdot\frac{\partial \varepsilon}{\partial x_j} = \frac{\partial}{\partial x_j}\left[\left(\nu + \frac{\nu_t}{\sigma_\varepsilon}\right)\frac{\partial \varepsilon}{\partial x_j}\right] + C_{1\varepsilon}\cdot\frac{\varepsilon}{k}\cdot\nu_t\left(\frac{\partial\overline{u_i}}{\partial x_j} + \frac{\partial\overline{u_j}}{\partial x_i}\right)\frac{\partial\overline{u_i}}{\partial x_j} - C_{2\varepsilon}\frac{\varepsilon^2}{k} + [(C_{1\varepsilon} - C_{2\varepsilon})\cdot\alpha_b + 1]\cdot G_b\cdot\frac{\varepsilon}{k} + S_\varepsilon \tag{6}$$

where $C_{1\varepsilon}$ and $C_{2\varepsilon}$ are constants; and σ_k and σ_ε are the turbulent Prandtl numbers for k and ε, respectively. The constants used in the k - ε model are taken directly from Launder and Spalding (1974) as (C_μ, σ_k, σ_ε, $C_{1\varepsilon}$, $C_{2\varepsilon}$) = (0.09, 1.0, 1.3, 1.44, 1.92). The coefficient α_b is optimized here as 1 (for details see Sogachev et al. (2012)). The production of turbulent kinetic energy by buoyancy (G_b) is expressed as follows (Sogachev et al., 2002):

$$G_b = -\frac{\nu_t}{\mathrm{Pr}_t}\cdot\beta\cdot g\cdot\left(\frac{\partial T}{\partial x_i} + \gamma_a\right) \tag{7}$$

S_u, S_T, S_q,S_k and S_ε are source terms considering the vegetation effect, which will be explained in Section 2.3.

2.3. Source terms modeling vegetation

The source term of momentum (Eq. (1)) is the function of the drag coefficient (C_d) and the *LAD*, defined as the total one-sided leaf area (m^2) per unit volume (m^3) (Raupach and Shaw, 1982; Weiss et al., 2004):

$$S_u = -C_d\cdot LAD\cdot\overline{u_i}\cdot|U| \tag{8}$$

where $|U|$ is the wind speed.

The source term for heat transfer (Eq. (2)) is as follows (Sogachev et al., 2002):

$$S_T = LAD_H\cdot g_{ha}\cdot(T_l - T) \tag{9}$$

where LAD_H is the total leaf surface area density taking part in the heat exchange with the surrounding air. In general, the relationship between *LAD* and LAD_H depends on the vegetation type. According to Campbell and Norman (1988), LAD_H= 2.7•*LAD* is for coniferous, and LAD_H= 2•*LAD* is for deciduous vegetation, and here we use 2•*LAD*. T_l is the leaf surface temperature. g_{ha} is an integral exchange coefficient for heat between the canopy air and photosynthetic surfaces, which is expressed as follows (Sogachev et al., 2005):

$$g_{ha}=1.4\cdot C_h\sqrt{|\overline{U}|/D} \tag{10}$$

where C_h = 0.135 m/s$^{0.5}$ is the proportionality factor. For applications in outdoor environments, a factor of 1.4 is used. D is the characteristic dimension of the leaf (0.72 times its width for the maize) (Campbell and Norman, 1988); here, we use the value of 0.05 (m) based on our field observation.

The source term of humidity (Eq. (3)) is defined as (Sogachev et al., 2002):

$$S_q = LAD_q\cdot g_q\cdot(q_l - q) \tag{11}$$

where LAD_q is the total leaf surface area density taking part in the water vapor exchange with the surrounding air. We assume $LAD_q = LAD_H$ (Campbell and Norman, 1988). g_q is an integral exchange coefficient for water vapor between the canopy air and photoelement surfaces, which is expressed as follows (Sogachev et al., 2005):

$$g_q = \frac{1}{r_{qa} + r_{qs}} = \frac{1}{\frac{1}{g_{qa}} + \frac{1}{g_{qs}}} \tag{12}$$

where r_{qa} and r_{qs} and g_{qa} and g_{qs} are the resistance and conductance of the leaf boundary layer and stomata, respectively.

$$g_{qa}=1.4\cdot C_v\sqrt{|\overline{U}|/D} \tag{13}$$

where $C_v = 0.147$ m/s$^{0.5}$ is the proportionality factor. g_{qs} is taken as 0.017 m/s for open maize leaves and 0.003 m/s is for closed maize leaves.

The source terms of turbulent kinetic energy (k) (Eq. (5)) and its dissipation rate (ε) (Eq. (6)) are specified as (Sogachev, 2009):

$$S_k = 0 \tag{14}$$

$$S_\varepsilon = 12(C_{2\varepsilon} - C_{1\varepsilon})\cdot C_\mu^{1/2}\cdot C_d\cdot LAD\cdot|U|\cdot\varepsilon \tag{15}$$

2.4. Radiation and energy balance equations of the canopy and soil

The air temperature and humidity can be obtained by iteratively solving the CFD governing equations. The leaf surface temperature (T_l) and humidity (q_l) are obtained by constructing the radiation transfer and energy balance equations in this model.

2.4.1. Radiation parameterization

We divide the vegetation canopy into different layers, and the total energy approaching each layer within the vegetation canopy $R_{absl}(z)$ is the sum of downward short-wave radiative flux $Q(z)$, and downward $F^{\downarrow}_{LWR}(z)$ and upward $F^{\uparrow}_{LWR}(z)$ fluxes of thermal radiation:

$$R_{absl}(z) = Q(z) + F^{\downarrow}_{LWR}(z) + F^{\uparrow}_{LWR}(z) \tag{16}$$

where $Q(z)$ is determined from the short-wave radiative flux hitting the top of the vegetation using Beer-Lambert law (Ross and Nilson, 1967; Campbell and Norman, 1988):

$$Q(z) = Q_0\cdot\exp\left(-\eta\cdot\int_z^{z_{top}} LAD\cdot dz\right) \tag{17}$$

where $\eta = 0.78$ is the extinction coefficient, and Q_0 is the short-wave radiative flux hitting the top of the vegetation, we use the value of 400 W/m^2 based on our field observation, which is the daytime (7:00 - 18:00 of local time) average value of July, 2012 (Xu et al., 2019). We refer to Sogachev et al. (2002) for details full equations and parameterizations used for the estimation of the downward and upward fluxes of thermal radiation, which is $F^{\downarrow}_{LWR}(z)$ and $F^{\uparrow}_{LWR}(z)$ respectively.

2.4.2. Energybalance equations of the canopy

We assume a stationary leaf energy balance and that the dynamic thermal storage of heat in leaves can be neglected. The energy balance of the leaf is given as follows (Bruse and Fleer, 1998; Yamada, 1982):

$$R_{absl} - L_{oel} - H_l - LE_l = 0 \tag{18}$$

L_{oel} is the emitted thermal radiation of leaves (Campbell and Norman, 1998):

$$L_{oel} = \delta_{LWR}\cdot\sigma\cdot T_l^4. \tag{19}$$

H_l is the sensible heat flux due to convective heat transfer from the leaf surface to the air, which is given as follows (Hicks et al., 1975):

$$H_l = \rho\cdot c_p\cdot g_{ha}\cdot(T_l - T) \tag{20}$$

where the specific heat capacity of air c_p is 1003.5 J/kg•K.

LE_l is the latent heat flux due to evapotranspiration, which is defined as follows:

$$LE_l = \lambda\cdot g_q\cdot(q_l - q) \tag{21}$$

To solve Eq. (18) with the term described by Eqs. (19), (20) and (21), respect to the leaf surface temperature we linearized the term with T_l^4 according to Deardorff (1978).

We commonly assume that the air specific humidity in stomatal cavities is the saturation vapor pressure at the leaf temperature (Cowan and Farquhar, 1977). Thus, the leaf surface humidity is defined as follows:

$$q_l = q_{sat}(T_l) = \frac{1.3318}{T_l}\exp\left[\frac{17.57(T_l - 273.15)}{241.9 + T_l - 273.15}\right] \tag{22}$$

2.4.3. Energybalance equations of the soil

The soil energy balance equation is given as follows (Yamada, 1982):

$$Rn_s = H_s + LE_s + G \tag{23}$$

where H_s is the sensible heat flux due to convective heat transfer from soil to air, LE_s is the soil latent heat flux due to evapotranspiration, and G is the heat conduction in the soil, which is given as $G = 1/3\bullet H_s$ (Yamada et al., 1997). Then, the soil temperature is also solved according to Deardorff (1978)'s method.

3. Study area, field observations and numerical simulations

The oasis-desert ecosystem is a complex nonlinear system, and the oasis-desert interactions in the real scenario are influenced by many factors, such as weather conditions, land surface hydrothermal conditions and vegetation patterns, oasis size and human activities. Moreover, oasis-desert microclimate characteristics often occur simultaneously. In order to investigate the complex oasis-desert interactions and the impact factors of the microclimate effects, we firstly designed a semisynthetic and idealized oasis-desert system to mimic the Zhangye oasis-desert area and introduced in Section 3.1. For ensuring the simulation results are consistent with the reality, the size of the system, the associated land surface hydrothermal conditions and vegetation covers were adopted from remote sensing and field observational evidence of the field campaign during the growing season, which is described in Section 3.2. The details of the numerical simulations were also shown in Sections 3.3 and 3.4.

3.1. The oasis-desert system and field campaign

The Zhangye oasis-desert area (37°28′39°57′N, 97°20′102°12′E) is located in the second largest inland river basin, the Heihe River Basin (HRB), in northwestern China, which is along the Silk Road Economic Belt. In particular, 95% of the cultivated land, 91% of the population and 89% of the gross national product of the HRB are concentrated in the Zhangye artificial oasis. Thus, investigating the microclimate effects in the Zhangye oasis-desert interactive ecosystem is significant to regional socioeconomic development and can also serve as a reference for other oasis-desert environments in semi-arid regions along the Silk Road (Chu et al., 2005; Li et al., 2016).

The Zhangye oasis-desert area experiences a typical temperate continental arid climate with an average elevation of 1770 m. The annual average relative humidity is 52%, the annual average air temperature is 7.3 °C, and the annual average precipitation is approximately 130.4 mm. The average annual evaporation is 2002.5 mm (statistics from 1971 to 2000). The Zhangye oasis is surrounded by multiple deserts (the Shenshawo Sandy Desert is to the east, the Bajitan Gobi is to the west, the Huazhaizi Desert steppe is to the south and the Badain Jilin Desert is to the north), and each has individual but

interacting characteristics (Cheng et al., 2014). Irrigated farmlands in the artificial oasis are distributed along the river course and divided into small patches by roads, windbreakers/shelterbelts, artificial canals and residential areas (Liu et al., 2016). To investigate the oasis-desert interactions, a field campaign, the "HiWATER-MUSOEXE" (Heihe Watershed Allied Telemetry Experimental Research, Multi-Scale Observation Experiment on Evapotranspiration over heterogeneous land surfaces) was conducted with the objectives to capture the 3-dimensional dynamic characteristics of heat and water vapor interactions between the land surface and atmosphere in the oasis-desert ecosystem (Li et al., 2013; Liu et al., 2018b; Xu et al., 2018).

The "HiWATER-MUSOEXE" experiment was conducted in the middle reaches of the HRB between May and September 2012 with two nested observation matrices of one 30 km × 30 km large experimental area (the oasis-desert ecosystem area) and one 5.5 km × 5.5 km kernel experimental area (the artificial oasis area) (Liu et al., 2016) (Fig. 4). In the 30 km × 30 km experimental region, the observation system includes one superstation (named Daman superstation) equipped with two EC (eddy covariance systems) sets (at the heights of 4.5 m and 34 m) and seven layers (at the heights of 3 m, 5 m, 10 m, 15 m, 20 m, 30 m and 40 m) of the meteorological gradient observation systems (within the oasis cropland) and four ordinary stations equipped with an eddy covariance system and an automatic meteorological station (around the oasis), with land surface desert and Gobi desert (37%), cropland and orchard (31%), residential area and roads (28%), wetlands and rivers (1%) and shelterbelts (3%). In the 5.5 km × 5.5 km experimental region, there are 17 ordinary stations with maize (69%), residential area and roads (14%), shelterbelts (9%), vegetables (5%) and orchards (3%). Overall, there are 22 ECs, 8 LASs (large aperture scintillometers), and 21 AWSs (automatic meteorological stations) in the "HiWATER-MUSOEXE" experiment. Additionally, a wireless sensor network, airborne and satellite remote sensing, auxiliary parameter observations were also measured. More details about the "HiWATER-MUSOEXE" experiment can be found in Liu et al. (2018b) and Ma et al. (2018).

3.2. The observational evidences

The numerical simulations in the current study are designed using ground observations and remote sensing data. The observations of the Bajitan Gobi station located in the northwest of the oasis (represents the conditions of desert) and the Daman superstation located inside the oasis (represents the conditions of oasis) from May 12 to September 25, 2012, revealed the following. The daily air temperatures of the oasis and desert vary between 9.5–25.6 °C and 11.3–28.3 °C, with averages of 18.6 °C and 20.8 °C, respectively. The daily air specific humidities of the oasis and desert vary between 2.5–14.3 g/kg and 1.8–12.9 g/kg, with averages of 8.6 g/kg and 6.8 g/kg, respectively. The daily wind velocities of the oasis and desert vary between 0.9–4.1 m/s and 2.0–7.1 m/s, with averages of 1.8 m/s and 3.7 m/s, respectively. Taking the daily variation in the air temperature and specific humidity on July 14, 2012 as an example (Fig. 2), there is an air temperature inversion in the near-surface layer of the oasis beginning at 17:00, and the temperature inversion difference is up to 0.2 °C. Although no air humidity inversion was observed, the specific humidity of the oasis and desert increased from 15:00 to 18:30. The temperature inversion and specific humidity increased mainly due to oasis-desert interactions.

From the LST obtained based on data Enhanced Spatial and Temporal Adaptive Reflectance Fusion Model, through multi-source remote sensing data (MODIS and ASTER/ETM+) on July 10, 2012 (Ma et al., 2018), the LST of the desert is approximately 320 K, the residential areas are approximately 307 K, and the vegetable, orchard and cropland are approximately 300 K (Fig. 3a). From the soil moisture obtained by airborne remote sensing (PLMR, Polarimetric L-band Multibeam Radiometer), on July 10, 2012, the soil moisture of the desert is 0.08 cm^3/cm^3, the residential areas are approximately 0.13 cm^3/cm^3, and the vegetable, orchard and cropland are approximately 0.18–0.30 cm^3/cm^3 (Fig. 3b). The LST and soil moisture difference between the oasis and desert are approximately 20 K and 0.22 cm^3/cm^3, respectively. From the height of roughness elements and *LAD* estimated by the Airborne Laser Scanning (ALS) data on July 19, 2012, the average height and *LAD* of maize are 2 m and 3.14 m^2/m^3 (Fig. 3c), respectively, and maize represents the main lower landscape of the oasis. The greatest height and average *LAD* of the shelterbelts are 30 m and 0.60 m^2/m^3, respectively (Liu et al., 2018a).

3.3. Numerical simulations

In the current study, we set up a semisynthetic and idealized oasis-desert ecosystem as our modeling domain (Fig. 4a), in which an oasis is surrounded by deserts according to the oasis-desert area in the middle reaches of HRB. Zhang and Yu (2001) analyzed the size of 15 typical oases in the HRB, which demonstrated that most of the oases are between 10 and 20 km in size. Furthermore, an oasis with a size greater than 10 km has a greater impact on the atmosphere (Patton et al., 2005). The simulation domain is 70 km in the *x*-direction and 5 km in the *y*-direction, wherein the oasis and desert sizes are 10 km and 30 km, respectively. Such a domain is comparable to a typical oasis-desert area and ensures that the oasis-desert interactions can be stimulated. Balancing the computing cost and the expression of the land surface, we used the horizontal grid resolution of 50 m for the oasis area. The resolution expands as a ratio of 1.05 for the desert area. The atmosphere boundary layer height of oasis-desert area is about 1 - 1.5 km (Huang et al., 2008; Zhou et al., 2018). In order to ensure the development of turbulence flow, the simulation domain should set 3 - 5 times of ABL height (Patton et al., 2005); thus the simulation domain is 3.5 km in the vertical direction. The vertical grid resolution is 1 m below a 50 m height and expanded as a ratio of 1.02 between 50 m to 1 km and 1.05 above 1 km (Fig. 4b).

According to previous studies (Pielke, 2001; Xue et al., 2018), the weather conditions, land surface hydrothermal conditions and vegetation patterns affect the oasis-desert interactions. In the current study, five numerical simulations that based on the observational pieces of evidence explained in Section 3.2 to represent the realistic oasis-desert scenario (including 31 numerical cases) varying inlet wind speed, LST difference in oasis-desert, vegetation fraction and vegetation distributions inside the oasis are used to investigate the oasis-desert interactions in oasis-desert ecosystems. It is worth noting that all the numerical simulations are based on the observational records in sunny summer daytime, when the oasis - desert interactions are more prominent (Su and Hu, 1988; Wang et al., 2018). Table 1 summarizes the details of the five numerical simulations (31 cases).

(1) The basic numerical simulation

The basic numerical simulation (named DO_0, DO means desert-oasis, and 0 means 0 m/s wind speed) sets homogenous vegetation at the height of 2 m, *LAD* of 3.14 m^2/m^3 and vegetation fraction at 100% in the oasis area, which represents the maize cropland in the artificial oasis, and there is no vegetation in the two surrounding desert areas. The LST and soil moisture of the oasis and desert are 300 K and 320 K and 0.08 cm^3/cm^3 and 0.28 cm^3/cm^3, respectively. The initial wind speed is 0 m/s.

(2) Inlet wind speed simulation

The simulation varies the inlet wind speed to examine the oasis-desert interactions under different background winds. The two numerical cases are named DO_3 and DO_5 for the 10 m inlet wind speeds of 3 and 5 m/s.

(3) LST difference between the oasis and desert simulation

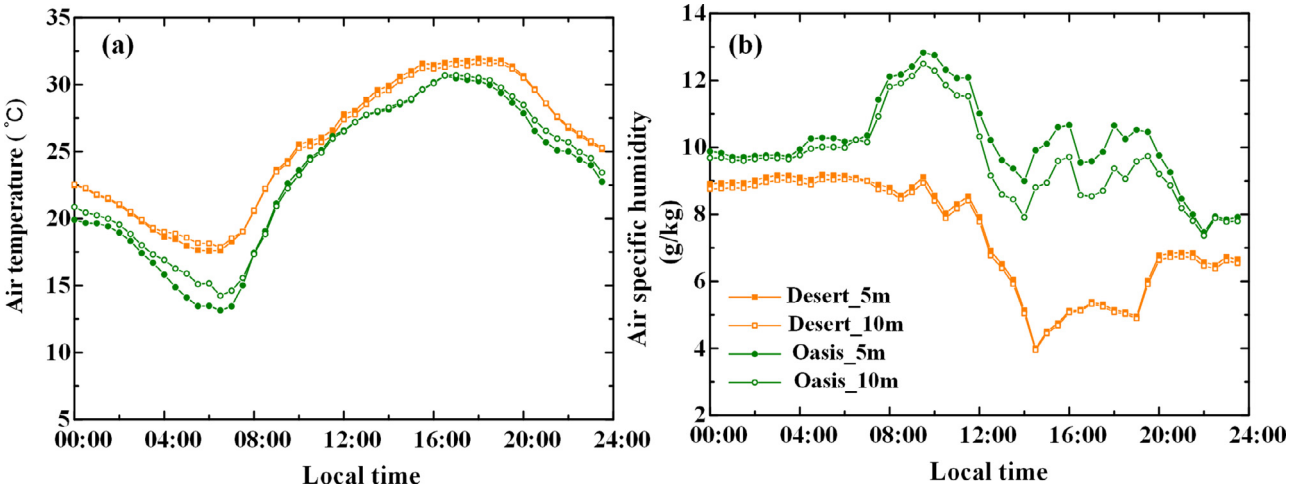

Fig. 2. Daily variations in (a) air temperature and (b) specific humidity on July 14, 2012.

The simulation varies the LST difference in the oasis-desert to examine the impact of the thermal contrast between the oasis and deserts on the oasis-desert interactions. This simulation includes 14 cases named DO_0_Ts (Ts means LST) for the oasis LST varying from 290–310 K (with a 2 K interval, and four additional cases around 300 K corresponding to 295, 297, 297, 299, 301 K). The initial wind speed is 0 m/s.

(4) Vegetation fraction simulation

The simulation varies the vegetation fraction of the oasis area and includes 11 cases named DO_0_fvc (fvc means vegetation fraction) for the vegetation fraction ranging from 30%−100% (with an interval of 10%). The initial wind speed is 0 m/s.

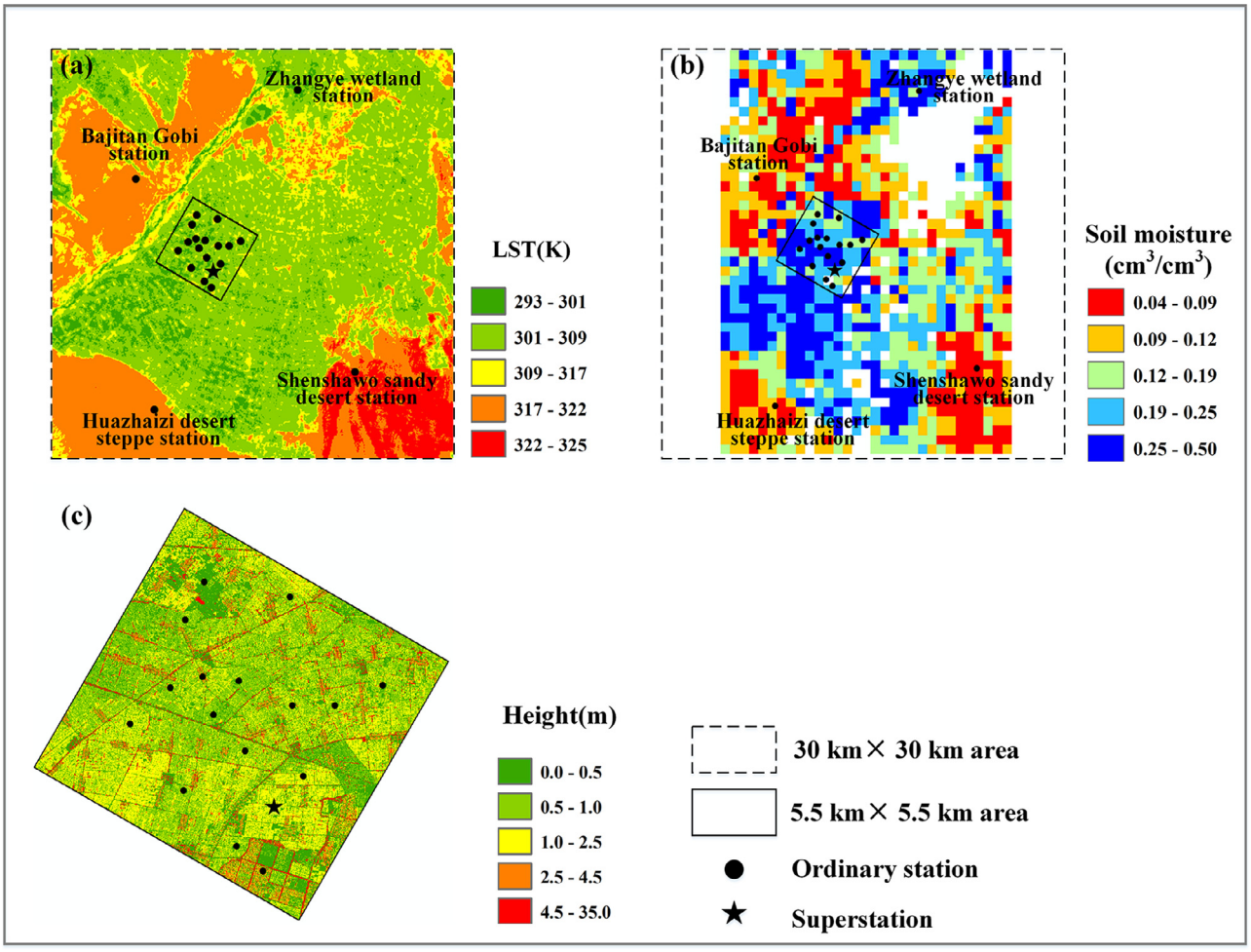

Fig. 3. The (a) LST (2012.07.10, resolution: 30 m); (b) soil moisture (2012.07.10, resolution: 700 m) and (c) height of roughness elements (2012.07.19, resolution: 1 m) of oasis-desert area.

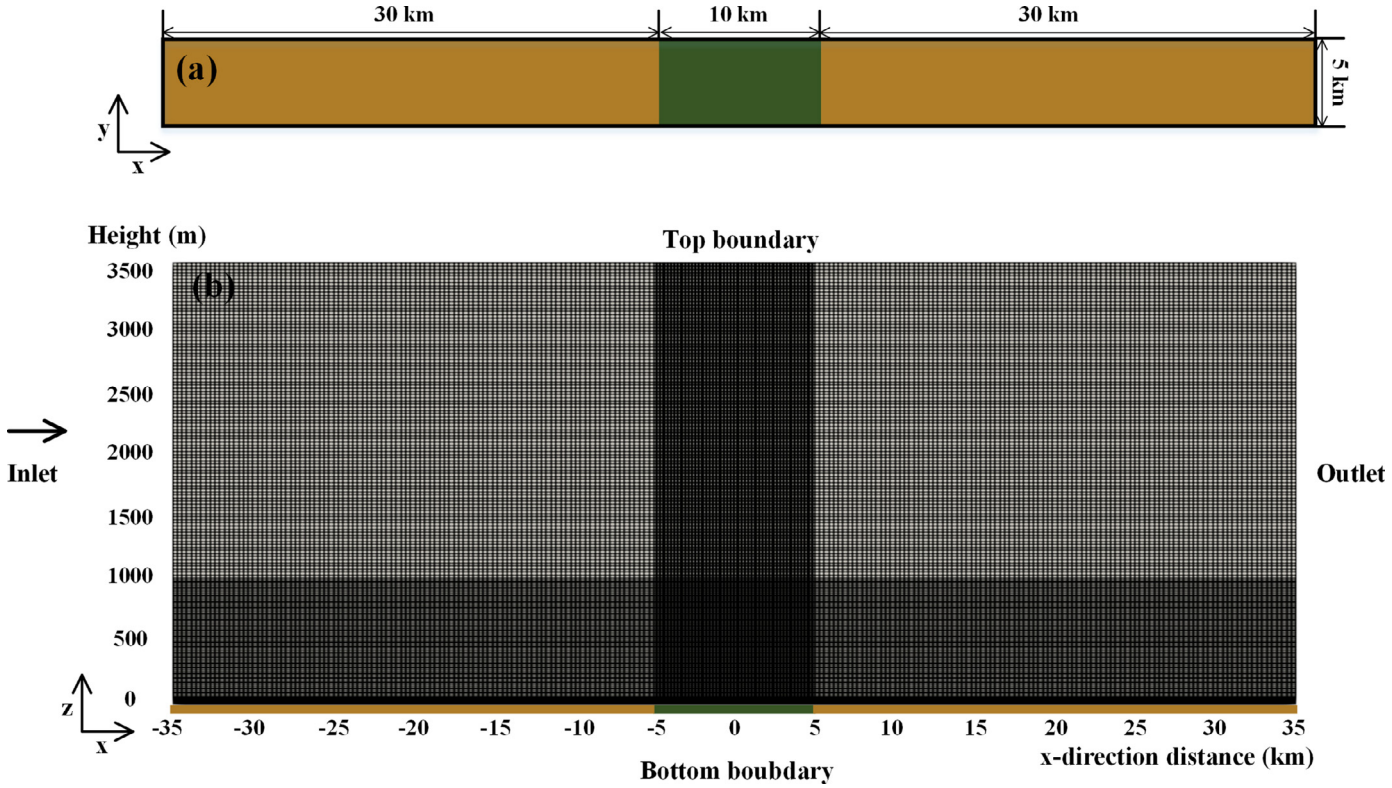

Fig. 4. Modeling domain: (a) The semisynthetic geometry of the oasis-desert area (brown and green patches represent desert and oasis, respectively) and (b) the mesh.

(5) Vegetation pattern simulation

In this simulation, we assume that there are two kinds of vegetation inside the artificial oasis: one is lower vegetation with a height of 2 m (representing the croplands in the oasis), and the other is higher vegetation with a height of 30 m (representing the shelterbelts in the oasis). According to the landscape of the Zhangye oasis, the lower vegetation covers approximately 80% of the land, and we set the area ratio of the lower and higher vegetation to design 3 cases for the different vegetation patterns named DO_0_V1, DO_0_V2 and DO_0_V3 (V is the vegetation pattern, and n = 1, 2, 3, 4 is the serial number) (Fig. 5b – d). For comparison with DO_0, we also design a case named DO_0_V4, where there is 100% coverage of higher vegetation at a 30 m height, and *LAD* is 0.60 m^2/m^3 (Fig. 5e). The initial wind speed is 0 m/s.

3.4. Numerical experimental configurations

In the current study, the inlet and outlet boundary conditions are set as periodic boundaries. To obtain the initial profiles of the variables at the periodic boundary, we first performed a precursor simulation that satisfies the aperiodic boundary of the initial profiles of the wind speed, air temperature and humidity fields. After obtaining convergence, the resulting flow fields are taken as the initial condition of the periodic boundary initializations. The inlet profiles of wind speed, turbulent kinetic energy and dissipation rate are as follows (Richards and Hoxey, 1993):

$$u(z) = \frac{u^*}{\kappa}\left[\ln\left(\frac{z + z_{0m}}{z_{0m}}\right)\right] \tag{24}$$

$$k = \frac{u_*^2}{\sqrt{C_\mu}} \tag{25}$$

$$\varepsilon = \frac{u_*^2}{\kappa(z + z_{0m})} \tag{26}$$

where κ is von Karman constant; z is the height, and z_{0m} is the aerodynamic roughness length, which is taken as 0.01 m.

The inlet profiles of temperature and specific humidity under the 1000 m height refer to the mesoscale model simulation results, which are expressed as follows:

$$T(z) = T - 0.0063 \cdot z \tag{27}$$

$$q(z) = q \cdot \exp(-0.8 \cdot 0.001 \cdot z) \tag{28}$$

The bottom boundary condition of temperature is adopted from the soil energy balance module, which has been described at Section 2.4.3. The lateral boundary conditions are also defined as periodic boundaries. To solve the governing equations and the turbulence closure, we use the QUICK (Quadratic Upstream Interpolation of the Convective Kinematics) algorithm for spatial discretization, which is a higher-order differencing scheme that accounts for the three-point upstream weighted quadratic interpolation of the cell phase values (Leonard, 1979). The SIMPLE (Semi-Implicit Method for Pressure-Linked Equations) algorithm is used to couple the velocity and pressure (Patankar,1981). In addition, to avoid solution errors resulting from incomplete convergence, a criterion on dimensionless residual errors was set to approximately $\leq 10^{-5}$ for each component. All the simulations were performed on Tianhe-II clusters (National Supercomputer Center, Guangzhou, China).

4. Results and discussions

4.1. The oasis-desert interactions

The background wind plays an important role in oasis-desert interactions. Fig. 6 shows the wind speed and air temperature simulated by cases DO_0, D0_3 and DO_5. Without the influence of background

Table 1
Summary of the numerical simulations.

Case	10-m inlet wind speed(m/s) (*U*)	Land Surface Temperature (K) (*Ts*)	Soil moisture (cm^3/cm^3)	Vegetation fraction (*fvc*)			Vegetation pattern (*Vn*)	Variate
			desert	oasis	desert	oasis		
DO_0	0	320	300	0.08	0.28	100%	*Lower vegetation	The basic numerical simulation
DO_3	3	320	300	0.08	0.28	100%	*Lower vegetation	Inlet wind speed
DO_5	5							
DO_0_Ts	0	320	290 /292 /294 /295 /296 /297 /298 /299 /300 /301 /302 /304 /306 /308/ 310	0.08	0.28	100%	*Lower vegetation	LST difference between oasis and desert
DO_0_fvc	0	320	300	0.08	0.28	30% /40% /50% /60% /70% /80% /90% /100%	*Lower vegetation	Vegetation fraction
DO_0_V1	0	320	300	0.08	0.28	100%	Staggered distribution of higher and lower vegetation	Vegetation distribution (Illustrated in Fig. 5)
DO_0_V2								
DO_0_V3							**Higher vegetation	
DO_0_V4								

* Lower vegetation (h = 2 m; LAD = 3.14 m^2/m^3; C_d = 0.20).
** Higher vegetation (h = 30 m; LAD = 0.60 m^2/m^3; C_d = 0.31).

wind, thermally induced local circulation is observed as two vortices colliding at the center of the oasis area (Fig. 6a). As a result, the airflow rises over the desert and sinks over the oasis. The airflow in the lower boundary layer converges and rises over the desert, while the upper level airflow diverges to the oasis. As the background wind increased to 3 m/s (case DO_3), the local circulation is gradually weakened by the high background wind, there are only weaken airflow sinking and rising over the cold and hot patch, respectively. The airflow is mainly transferred horizontally from desert to oasis. For the horizontal transport of dry and hot air from desert to oasis, there exists an oasis thermal internal boundary layer because of the hydrothermal differences between the oasis and desert (Fig. 6b). As the background wind increased to 5 m/s (case DO_5), the thermally derived local circulation diminished because of the sufficiently large background wind, and the airflow over the oasis-desert system is dominated by horizontal transfer. Only the dynamic internal boundary layer is derived from the oasis-desert contrasts in the aerodynamic roughness length of the underlying surfaces, which is due to the stronger drag force over the oasis area. Notably, the dynamic internal boundary layer always covers the oasis (Fig. 6c). Thus, we can conclude that the background wind has a significant impact on oasis-desert interactions, and the local circulation is more pronounced under calm conditions, what is consistent with previous studies (Zhang et al., 2014; Zhu et al., 2016; Wang et al., 2017).

4.2. Oasis-desert microclimate effects

The microclimate effects stimulated by the oasis-desert interactions result in the positive feedback that is beneficial to the maintenance and development of the oasis ecosystem (Su and Hu, 1988; Wu et al., 2003; Chu et al., 2005; Meng et al., 2012). In this section, we will explore and discuss the oasis-desert microclimate effects from the following aspects: the oasis cold-wet island effect, air humidity inversion effect within the surrounding desert and the oasis wind shield effect.

The significant hydrothermal differences between the oasis and desert cause the local circulation and the oasis thermal internal boundary layer under relatively calm conditions. In the upper atmospheric environment, the air density and pressure over the desert are higher than those over the oasis. This air density and pressure gradient drive dry and hot air over the desert, which flows toward the oasis, and the hot-dry air in the upper atmospheric environment overlies the cold-moist air near the oasis surface and forms a static thermal inversion layer. The transfer of energy from the desert to the oasis is beneficial for improving vegetation productivity and evapotranspiration. From the air temperature and specific humidity distributions in cases DO_0 and DO_3 (Fig. 7), the oasis is colder and moister than the surrounding deserts, which reflects the oasis cold-wet island effect. Comparing Fig. 7a (7c) and 7b (7d), when there is no background wind (case DO_0), the cold-wet island center is the same as the center of the oasis area; when there is weaker background wind (case DO_3), the cold-wet island center is moved to the downwind direction. The stability over the oasis is beneficial for the oasis stability mechanism; to some extent, it inhibits water vapor diffusion from the oasis to the atmosphere, increases the water-use efficiency, and positively affects the sustainable development of the oasis.

Furthermore, we analyze air temperature and specific humidity profiles over the oasis and desert areas, which are at the locations of x = 0 km (representing the oasis), x = −6 km (representing the upwind desert, which is about 1 km distance from the upwind edge of oasis) and x = 6 km (representing the downwind desert, which is about 1 km distance from the downwind edge of oasis) (Fig. 8). From the air temperature profiles of the oasis (at the location of x = 0 km), the thermal inversion is clearly observed (Fig. 8a and b). When the background wind is 0 m/s, the height of the thermal inversion layer is approximately 200 m, while it decreases to 100 m with a background wind of 3 m/s. We can conclude that the height and intensity of the cold-wet island effect are also reduced due to the increase in

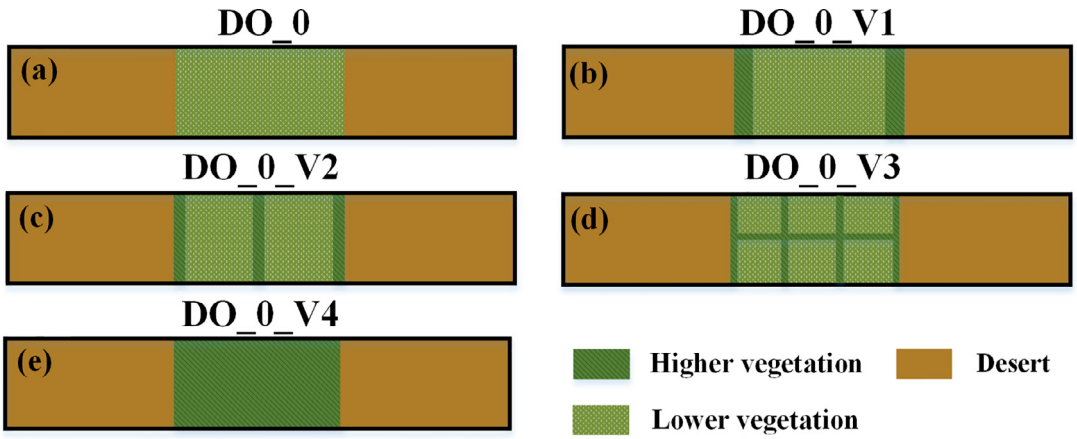

Fig. 5. Illustration of the numerical simulation with various vegetation distributions.

background wind.

When there is local circulation or an oasis thermal internal boundary layer under relatively calm conditions, the air density and pressure over the desert are smaller than that over the oasis in the near-surface boundary layer. The pressure difference drives moist and cold airflow from the oasis to the desert, resulting in a specific humidity inversion over the near-surface boundary layer of the surrounding deserts, which is known as the air humidity inversion effect. The transfer of water vapor from the oasis to the near-surface boundary layer of the desert positively affects the maintenance of desert vegetation. From the profiles of air specific humidity of the surrounding deserts (at the locations of $x = -6$ km and $x = 6$ km), there is an air humidity inversion over the desert (Fig. 8c and d). Furthermore, when increasing the background wind speed (case DO_3), the air humidity is only increasing and there is no air humidity inversion over the upwind desert; the air humidity inversion only occurred in the downwind desert. Thus, as the background wind increased, the intensity and height of the air humidity inversion were smaller and lower, which ranged from 0.5 g/kg (at a height of 8 m) to 0.3 g/kg (at a height of 3 m).

Furthermore, we take an example of wind speed profiles over the oasis and deserts simulated by cases DO_5 and DO_3 to further analyze dynamic internal boundary layer over the oasis due to the change in aerodynamic roughness length of the underlying surfaces from desert to oasis (Fig. 9). When the air moves from a flat upwind desert to the oasis with 2 m height homogenous vegetation, the wind profile is lifted and then drops off from oasis to desert. Since the kinetic energy of the airflow is reduced by the drag force of the vegetation over the oasis, the horizontal wind speed over the oasis is smaller than that over the deserts. Moreover, the wind speed over the downwind desert is smaller than that over the upwind desert, which means that the oasis has a "wind shield" effect. There is also an acceleration zone of wind speed above the vegetation (2–100 m), which was indicated by Liu et al. (2018a) when they investigated the wind shield effect over highly heterogeneous multiarray shelter belts. Fig. 9b shows that the wind speed over the oasis (at the location of $x = 0$ km) is slightly higher than the upwind desert (at the location of $x = -6$ km) above 80 m height when the background wind is 3 m/s (DO_3). The same phenomenon was also simulated by Zhang et al. (1998). The reason is that in the case of DO_3, there is a thermal inversion below the 100 m height. The static thermal inversion layer will suppress the momentum transmission above 100 m. From the aspect of oasis self-maintenance, the oasis "wind shield" effect prevents wind erosion in the desert and decreases the wind speed over the oasis. Moreover, the oasis "wind shield" effect moderates the background wind over the oasis, which is beneficial to the oasis-desert local circulation and further beneficial to the oasis cold-wet island effect and air humidity inversion effect within the surrounding desert.

4.3. Impact factors of oasis-desert microclimate effects

In the previous section, the oasis-desert microclimate effects caused by the oasis-desert interactions under different background wind conditions are discussed. It can be concluded that under calm conditions, the oasis-desert local circulation is clear, and the intensity of the oasis-desert microclimate effects is strong. In this section, we use the results of the simulations that change the thermal difference of oasis-desert land surface (case DO_0_Ts), vegetation fraction (case DO_0_fvc) and distribution (cases DO_0, DO_0_V1, DO_0_V2, DO_0_V3 and DO_0_V4) inside the oasis to further investigate the impact factors of oasis-desert microclimate effects. Notably, all the cases in this section are simulated with no background wind. We use the horizontal and vertical wind velocities, which are formed purely by the hydrothermal differences in oasis-desert, air temperature and air specific humidity over the oasis to qualify the intensity of oasis-desert interactions. In the current study, the horizontal and vertical wind speed is taken from the maximal value at $x = (-10)$ to (-5) km and $x = 5$ to 10 km (at the height of 10 m in the vertical), which represent the desert area. The air temperatures is taken from the minimal value at the $x = (-5)$ to 5 km (at the height of 10 m in the vertical), and the air specific humidity is taken from the maximal value at the $x = =(-5)$ to 5 km (at the height of 10 m in the vertical), which represent the oasis area. The larger horizontal and vertical wind velocities, the smaller air temperatures and larger air specific humidities over the oasis indicate strong oasis-desert interactions. Therefore, these conditions are more conducive to oasis self-maintenance and development.

4.3.1. Land surface thermal conditions between the oasis and desert

Fig. 10 shows that the LST difference in the oasis-desert is one of the main factors affecting oasis-desert interactions. The large LST difference in the oasis-desert produces larger horizontal and vertical wind velocities, which means stronger oasis-desert interactions (Fig. 10a). Additionally, a larger LST difference in the oasis-desert leads to a smaller air temperature over the oasis and more air specific humidity, which means a stronger oasis "wet-cold island" effect (Fig. 10b). Specifically, there is a threshold value of approximately 22 K. In other words, when the LST difference is more than 22 K, the oasis-desert interactions are no longer sensitive to the LST difference. Usually, irrigation of the oasis is most important for maintaining the oasis due to less precipitation (Xue et al., 2018). Because irrigation will increase soil moisture, one way to increase the LST difference in oasis deserts is to intensify irrigation. Considering that water resources in arid and semi-arid areas are scarce yet valuable, our findings suggest to support the LST difference of the oasis-desert at approximately 22 K through managed practice, such as drip irrigation, to reduce unnecessary consumption of water resources.

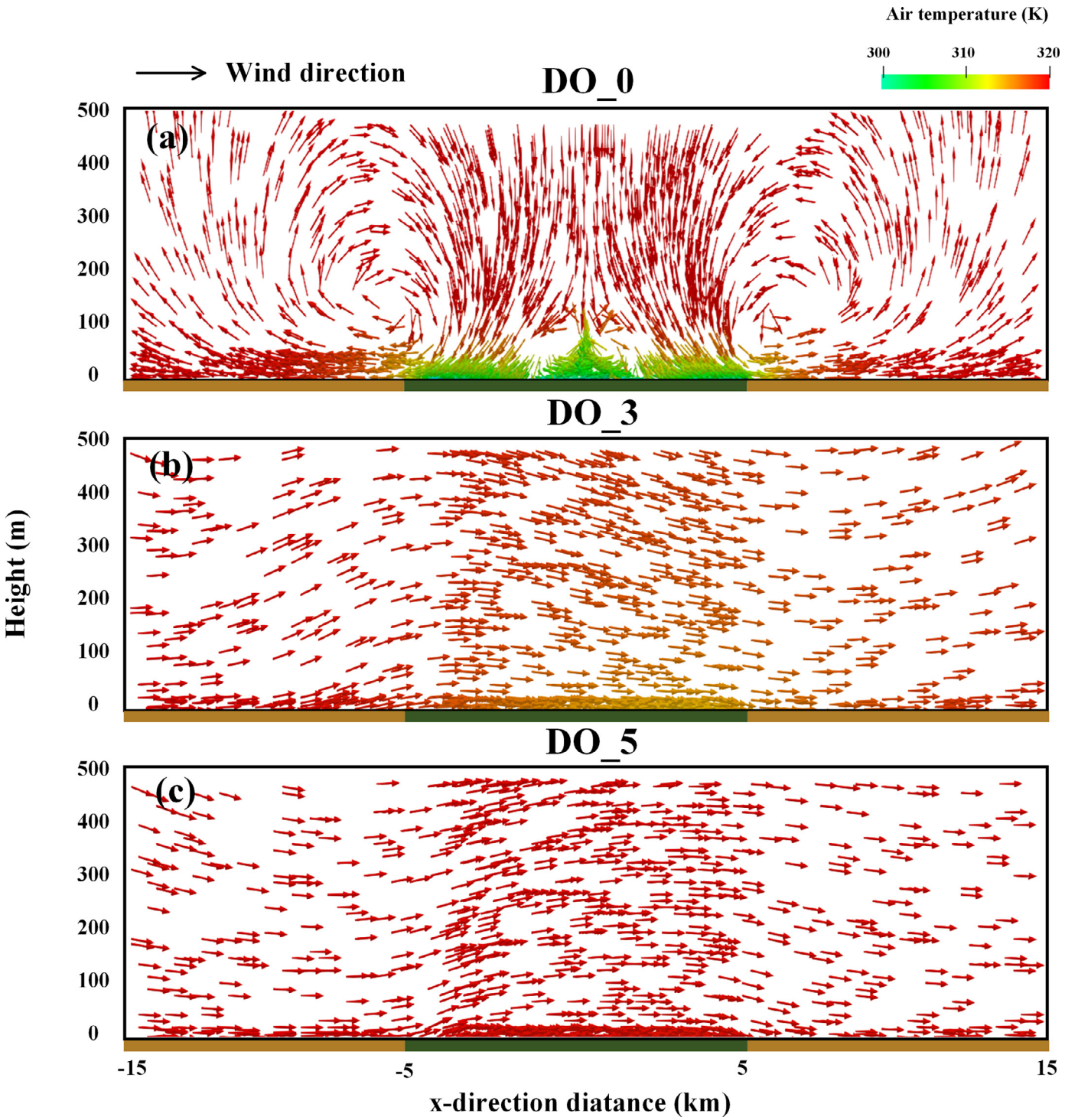

Fig. 6. Vertical cross-sections of wind direction and air temperature for cases (a) DO_0; (b) DO_3 and (c) DO_5.

4.3.2. Vegetation fraction

Fig. 11 shows that the vegetation fraction of the oasis is also one of the main factors affecting oasis-desert interactions. Fig. 11a shows that the vegetation fraction has little effect on the vertical wind speed but a greater impact on the horizontal wind speed with a positive ratio. There is a threshold vegetation fraction value of 70%, which means that when the vegetation fraction is larger than 70%, the horizontal wind speed is less affected by the vegetation fraction. The oasis with the 70% vegetation fraction is beneficial to the oasis-desert microclimate effects. Fig. 11b shows that when the vegetation fraction is less than 60%, the vegetation fraction has little effect on the air temperature of the oasis. Thus, as the vegetation fraction increases, the intensity of the oasis cold island effect gradually increases. When the vegetation fraction is less than 70%, the air specific humidity increases with increasing vegetation fraction; when it is 70%, the air specific humidity reaches a certain peak; and when it exceeds 70%, the influence of the air specific humidity is no longer obvious. In summary, it can be inferred that keeping the vegetation fraction of the oasis within the range of 60%−70% is beneficial to the effects of the oasis-desert microclimate. However, in recent decades, many oases have been threatened by desertification, abandoned farming and the expansion of residential areas due to human activities (Wang et al., 2008). Thus, we should pay attention to

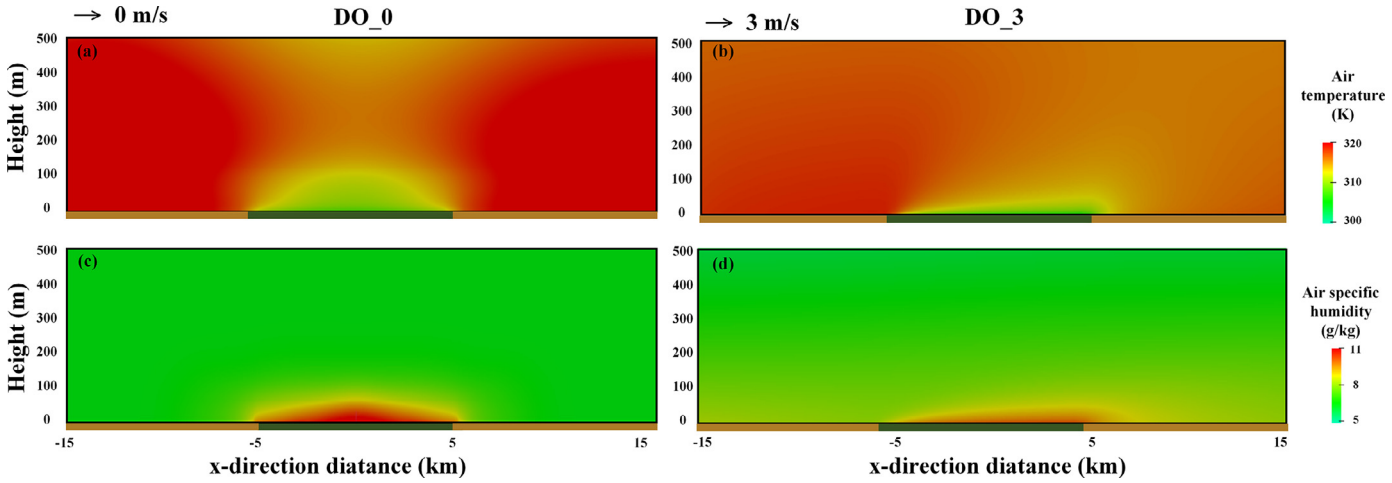

Fig. 7. Contour plots of air temperature and specific humidity (a) and (c) with no background wind (case DO_0); (b) and (d) with 3 m/s inlet wind speed (case DO_3).

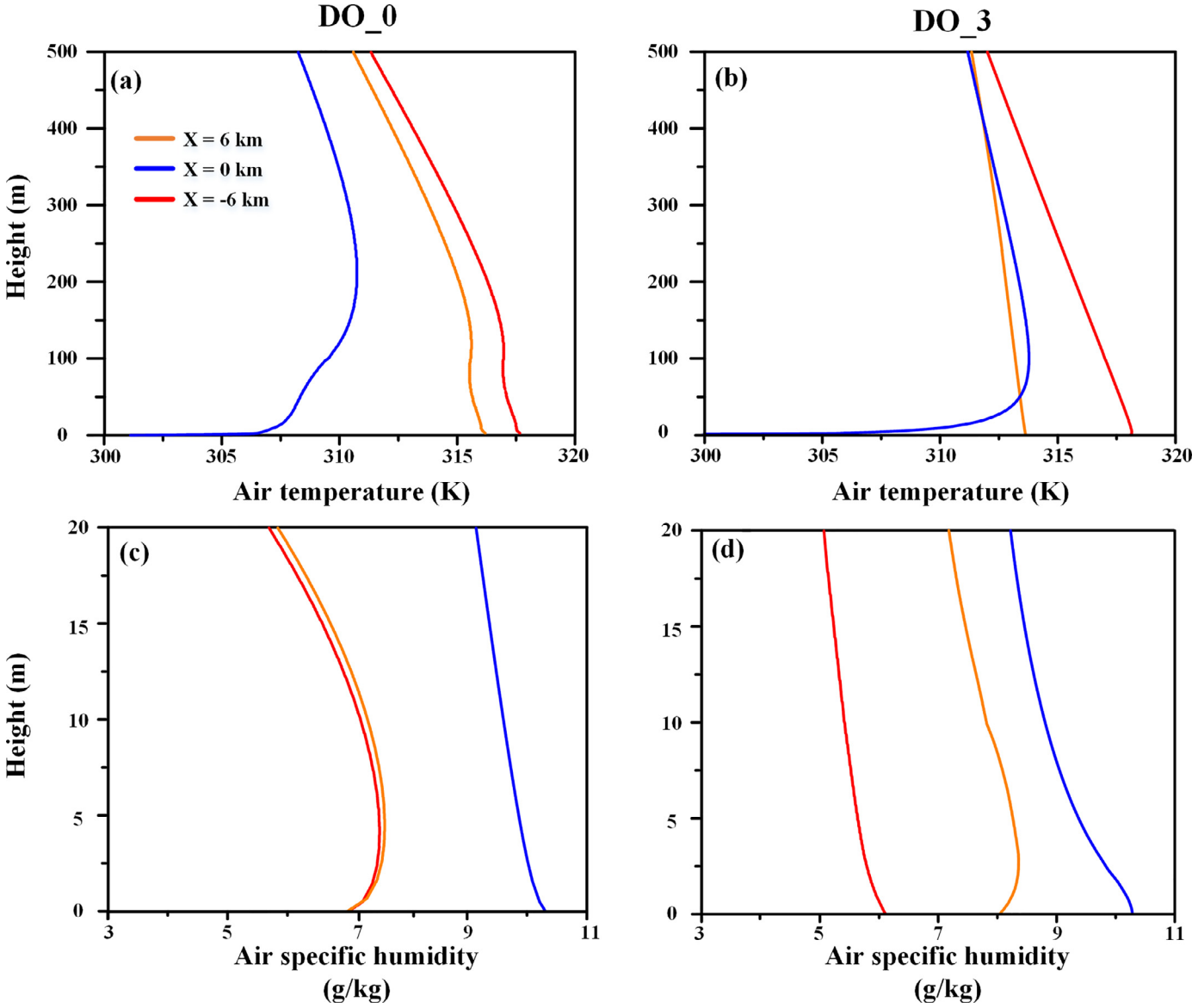

Fig. 8. Air temperature and specific humidity profiles at selected locations in the oasis and desert areas for case DO_0 ((a) and (c)) and case DO_3 ((b) and (d)).

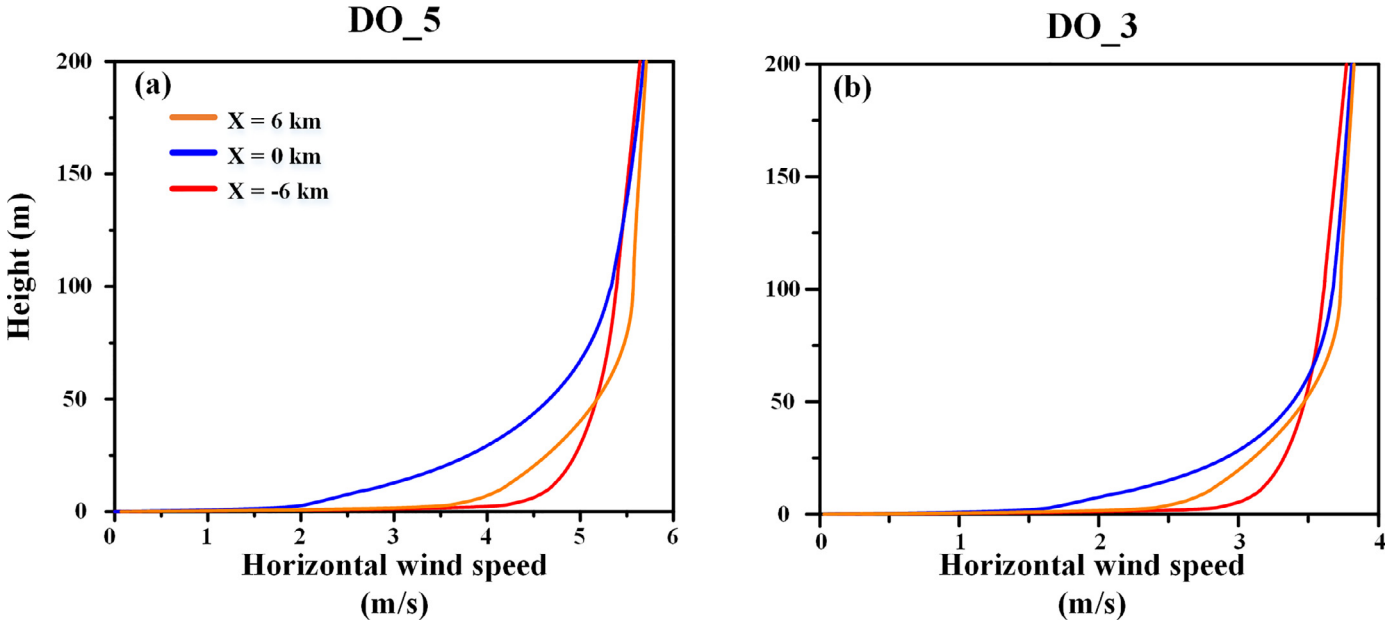

Fig. 9. Horizontal wind speed profiles in the oasis and desert areas for (a) DO_5 and (b) DO_3.

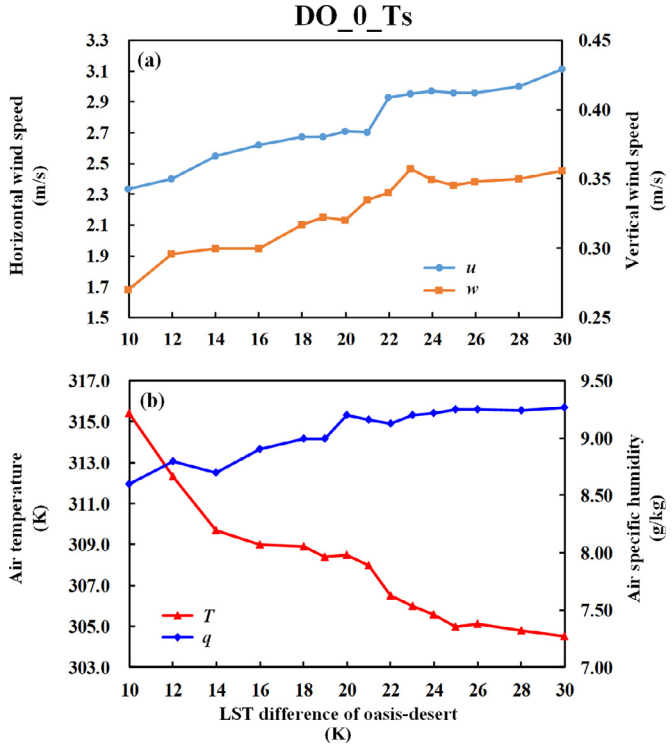

Fig. 10. The impact of the LST difference between the oasis and desert.

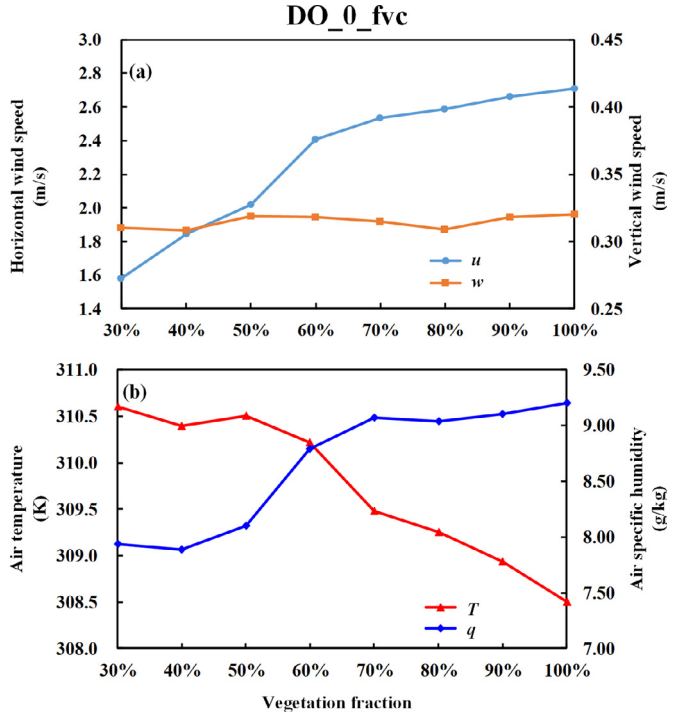

Fig. 11. The impact of the vegetation fraction within an oasis on the oasis-desert interactions.

the intensification of oasis desertification and maintain the vegetation fraction of oases at a 60% minimum.

4.3.3. Vegetation patterns

The actual artificial oasis is mainly distributed in the lower croplands and higher shelterbelts. In this section, the impact of higher and lower vegetation patterns within oasis on oasis-desert interactions will be analyzed. Fig. 12 shows the variation in air temperature within the oasis under different vegetation patterns. The oasis covered with the higher vegetation shows the most obvious cold island effect (case DO_0_V4, Fig. 12e), while the case DO_0 with the lower vegetation has the weakest cold island effect (case DO_0, Fig. 12a). Figs. 12b – d (cases DO_0_V1, DO_0_V2 and DO_0_V3) show that different vegetation patterns of lower and higher vegetation alter the wind direction and reduce the air temperature, which plays an important role in the oasis-desert interactions. The variation in air specific humidity is similar to the air temperature; here, we do not show the contours of air specific humidity, but further statistics show the indicators of the oasis-desert interaction intensity (Table 2). Case DO_0_V4 has the strongest oasis-desert microclimates due to the larger horizontal and vertical wind velocities, lower air temperature and higher air specific humidity. The case DO_0_V3 is in the second. However, integrated ecological and economic benefits of the oasis, the vegetation patterns of case DO_0_V3

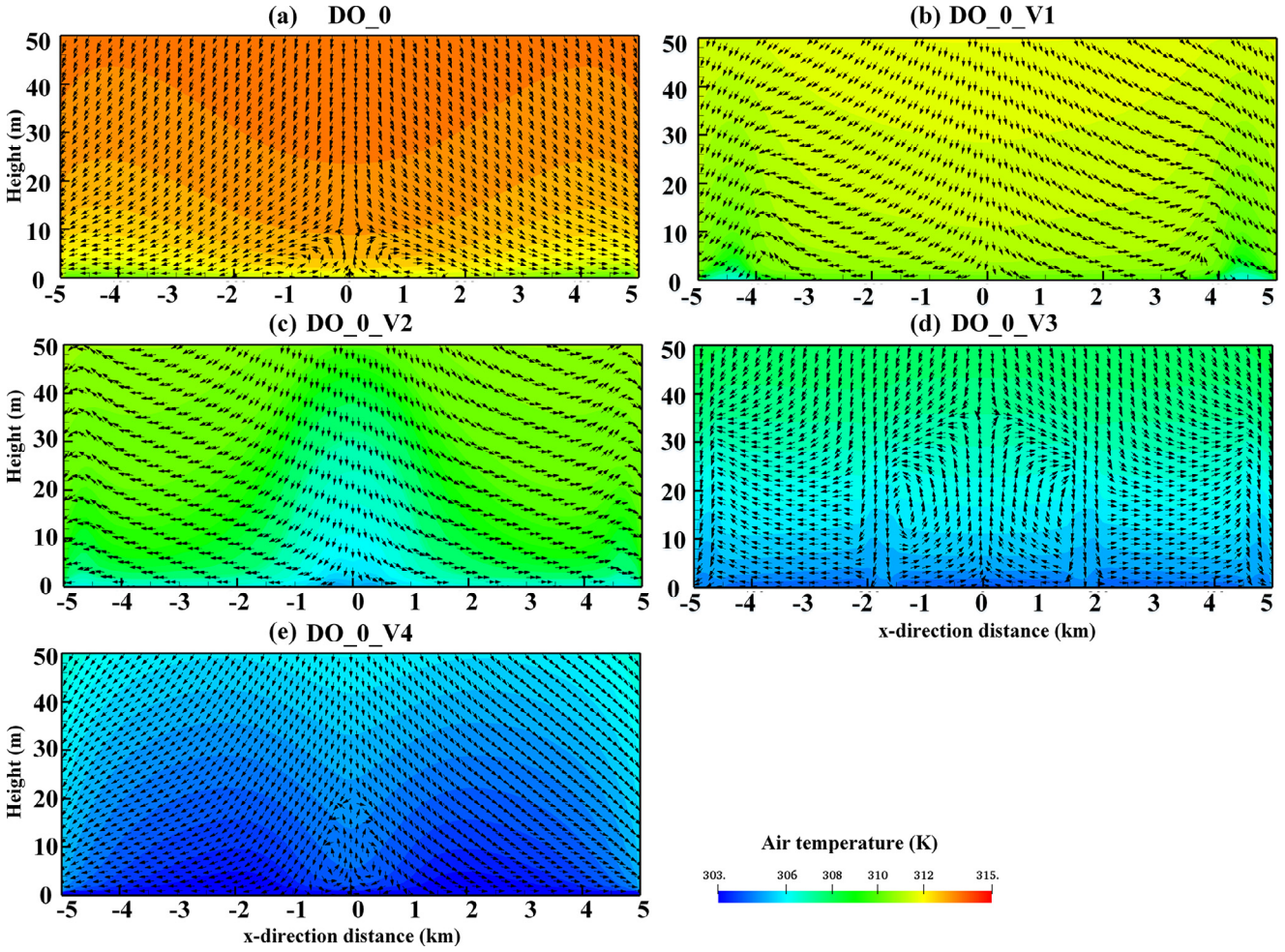

Fig. 12. Variations in wind speed and air temperature within the oasis under different vegetation patterns.

Table 2
Summary of the intensities of oasis-desert interactions.

	DO_0	DO_0_V1	DO_0_V2	DO_0_V3	DO_0_V4
u_{max} (m/s)	2.71	2.65	2.73	2.58	3.22
w_{max} (m/s)	0.320	0.343	0.335	0.344	0.343
T_{min} (K)	308.5	308	306.2	305.1	303.5
q_{max} (g/kg)	9.2	11.5	11.3	12.2	14.1

*Greener indicates stronger oasis-desert interactions; redder indicates weaker oasis-desert interactions.

with staggered croplands and shelterbelts surrounding the oasis are more reasonable. Thus, building shelterbelts around the oasis can create a buffer zone for reducing the wind speed over the oasis, which is beneficial to the oasis-desert microclimate effect. Moreover, croplands and shelterbelts in the oasis can reduce soil evaporation over the oasis and resist sandstorms (Meng et al., 2009).

The threshold values of the impact factors of oasis-desert microclimate effects are qualitative from the current simulation, since the grid resolution of the simulation domain may lead to different absolute values of the impact factors. However, these results seem plausible based on our observations: the LST difference of Zhangye oasis-desert area is approximately 22 K during 2016 and 2018, and the vegetation fraction of Zhangye oasis is up to 60%−70%.

5. Conclusion

In this study, we developed an improved CFD model considering the buoyancy and vegetation effects (the radiation distributions within vegetation and the energy balance of leaf and soil) to simulate the interactions between the vegetation canopy and atmospheric boundary layers. Then, we simulated the atmospheric boundary layer flows, air temperature and humidity over an idealized oasis-desert system based on observational evidence from the HiWATER-MUSOEXE experiment. Based on the simulations, we analyzed the impacts of weather conditions, hydrothermal conditions, the vegetation fraction and vegetation patterns within the oasis on the oasis-desert microclimate effects. Additionally, we discussed the oasis self-maintenance mirrored by the oasis microclimate effects. The main conclusions are summarized as follows.

(1) The oasis-desert interactions conducted by their contrasts in aerodynamic roughness length and hydrothermal conditions are significantly affected by background wind conditions. Without the background wind, thermally induced oasis-desert local circulation begins to appear. Under the low wind speed condition, there is an oasis thermal internal boundary layer. When the background wind is sufficiently large, there is only an oasis dynamic internal boundary layer caused by the aerodynamic roughness length contrast between oasis and desert, while the oasis-desert interactions due to the hydrothermal conditions contrast are interrupted.
(2) The oasis-desert interactions lead to a series of microclimate effects, including the cold-wet island effect, air humidity inversion effect

and “wind shield” effect. Under relatively calm conditions, the oasis-desert interactions form a static thermal inversion layer, which suppresses the loss of evaporation and stimulates the transport of water vapor to the desert. Such stability in the oasis results in the oasis cold-wet island effect and air humidity inversion effect within the surrounding desert. As the background wind increased, the height and intensity of the cold-wet island effect were reduced. Meanwhile, the center of the cold-wet island is moved in the downwind direction. Moreover, when the background wind speed is increased, the intensity and height of the air humidity inversion are reduced. In general, the air humidity inversion effect within the surrounding desert exits in the downwind desert.

(3) The hydrothermal condition difference between the oasis and desert, the vegetation fraction and distribution patterns impact the oasis-desert microclimate effects. We found that the intensity of oasis-desert interactions is increasing with the LST difference in the oasis-desert, and the threshold LST difference is approximately 22 K. The oasis-desert interactions gradually strengthen with the increase in vegetation fraction within the oasis, and the threshold vegetation fraction is about 60%. Integrated ecological and economic benefits of the oasis, the staggered distribution of croplands and shelterbelts surrounding the oasis that creates a buffer zone for reducing the wind speed, limits the loss of evaporation and prevents sandstorms in the oasis. Thus, we should support these impact factors under the threshold values to maintain the microclimate effects and ensure the sustainability of oasis-desert ecosystems.

Future studies should improve the vegetation parameterizations, radiative transfer and energy balance mechanics of the CFD model. Grid tests will be conducted to verify the threshold values of impact factors. Besides, CFD simulations will be performed over realistic heterogeneous oasis-desert areas to fundamentally understand the detailed structures of the atmosphere boundary layer over the oasis-desert areas and the small-scale energy and water vapor exchange between the oasis and desert, such as the diurnal variation in oasis-desert interactions, the impact of irrigation on the oasis-desert interactions.

Acknowledgements

This work is funded by the Strategic Priority Research Program of the Chinese Academy of Sciences (Grant no. XDA20100101), the National Natural Science Foundation of China (41531174) and Special Program for Applied Research on Super Computation of the NSFC-Guangdong Joint Fund (the second phase). We appreciate the anonymous reviewers for their constructive comments. We also acknowledge Dr. Ebba Dellwik and Dr. Paul van der Laan (both at DTU Wind Energy, Denmark) for their insightful and useful reviews of this manuscript.

References

Anderson, J.D., Wendt, J., 1995. Computational FluidDynamics 206 McGraw-Hill, New York.

Bavel, V., 1967. Changes in canopy resistance to water loss from alfalfa induced by soil water depletion. Agricult. Meteorol. 4 (3), 165–176.

Bruse, M., Fleer, H., 1998. Simulating surface–plant–air interactions inside urban environments with a three dimensional numerical model. Environ. Model. Softw. 13 (3–4), 373–384. https://doi.org/10.1016/S1364-8152(98)00042-5.

Campbell, G.S., Norman, J.M., 1998. An Introduction to EnvironmentalBiophysics. Springer Science and Business Media.

Chen, Q., Jia, L., Hutjes, R., Menenti, M., 2015. Estimation of Aerodynamic Roughness Length over Oasis in the Heihe River Basin by Utilizing Remote Sensing and Ground Data. Remote Sens. (Basel) 7 (4), 3690–3709. https://doi.org/10.3390/rs70403690.

Cheng, G., Li, X., Zhao, W., Xu, Z., Feng, Q., Xiao, S., Xiao, H., 2014. Integrated study of the water-ecosystem-economy in the Heihe River Basin. Natl. Sci. Rev. 1 (3), 413–428. https://doi.org/10.1093/nsr/nwu017.

Chu, P.C., Lu, S., Chen, Y., 2005. A numerical modeling study on desert oasis self-supporting mechanisms. J. Hydrol. (Amst) 312 (1–4), 256–276. https://doi.org/10.1016/j.jhydrol.2005.02.043.

Cowan, I.R., Farquhar, G.D., 1977. Stomatal function in relation to leaf metabolism and environment. In Symposia of the Society for Experimental Biology 31, 471.

...Crétaux, J.F., Calmant, S., Romanovski, V., Shabunin, A., Lyard, F., Bergé-Nguyen, .M.., Perosanz, F., 2009. An absolute calibration site for radar altimeters in the continental domain: lake Issykkul in Central Asia. J. Geod. 83 (8), 723–735. https://doi.org/10.1007/s00190-008-0289-7.

De Azagra, A.M., Mongil, J., Rojo, L., 2004. Oasification: a forest solution to many problems of desertification. For. Syst. 13 (3), 437–442.

Deardorff, J.W., 1978. Efficient prediction of ground surface temperature and moisture, with inclusion of a layer of vegetation. J. Geophys. Res. Oceans 83 (C4), 1889–1903.

...Fernando, H.J.S., Mann, J., Palma, J.M.L.M., Lundquist, J.K., Barthelmie, R.J., Belo-Pereira, M., Klein, P.M., 2019. The Perdigao: peering into microscale details of mountain winds. Bull. Am. Meteorol. Soc. 100 (5), 799–819. https://doi.org/10.1175/BAMS-D-17-0227.1.

Foken, T., Aubinet, M., Finnigan, J.J., Leclerc, M.Y., Mauder, M., Paw, U., K.T., 2011. Results of a panel discussion about the energy balance closure correction for trace gases. Bull. Am. Meteorol. Soc. 92 (4), ES13–ES18. https://doi.org/10.1175/2011BAMS3130.1.

Georgescu, M., Moustaoui, M., Mahalov, A., Dudhia, J., 2011. An alternative explanation of the semiarid urban area “oasis effect”. J. Geophys. Res. 116 (D24). https://doi.org/10.1029/2011JD016720.

Hao, X., Li, W., Deng, H., 2016. The oasis effect and summer temperature rise in arid regions - case study in Tarim Basin. Sci. Rep. 6, 35418.

Harrison, P., Pearce, F., 2000. AAAS Atlas of PopulationEnvironment. Univ of California Press.

Hicks, B.B., Hyson, P., Moore, C.J., 1975. A study of eddy fluxes over a forest. J. Appl. Meteorol. 14 (1), 58–66. https://doi.org/10.1029/2011JD016720.

Huang, J., Lee, X., Patton, E.G., 2008. A modelling study of flux imbalance and the influence of entrainment in the convective boundary layer. Boundary Layer Meteorol. 127 (2), 273–292. https://doi.org/10.1007/s10546-007-9254-x.

Launder, B., Spalding, D. (1974). Computer Methods in Applied Mechanics and Engineering, 3(2), 269–289.

...Lee, X., Gao, Z., Zhang, C., Chen, F., Hu, Y., Jiang, W., Zeng, Z., 2015. Priorities for boundary layer meteorology research in China. Bull. Am. Meteorol. Soc. 96 (9), ES149–ES151. https://doi.org/10.1175/BAMS-D-14-00278.1.

Leonard, B.P., 1979. A stable and accurate convective modelling procedure based on quadratic upstream interpolation. Comput. Methods Appl. Mech. Eng. 19 (1), 59–98. https://doi.org/10.1016/0045-7825(79)90034-3.

Li, X., Cheng, G., Liu, S., Xiao, Q., Ma, M., Jin, R., Wen, J., 2013. Heihe watershed allied telemetry experimental research (HiWATER): scientific objectives and experimental design. Bull. Am. Meteorol. Soc. 94 (8), 1145–1160. https://doi.org/10.1175/BAMS-D-12-00154.1.

Li, X., Yang, K., Zhou, Y., 2016. Progress in the study of oasis-desert interactions. Agric. For. Meteorol. 230, 1–7. https://doi.org/10.1016/j.agrformet.2016.08.022.

Liu, R., Liu, S.M., Yang, X.F., Lu, H., Pan, X.D., Xu, Z.W., Ma, Y.F., Xu, T.R., 2018a. Wind dynamics over a highly heterogeneous oasis area: an experimental and numerical study. J. Geophys. Res. 123, 8418–8440. https://doi.org/10.1029/2018JD028397.

Liu, S.F., Yue, X., Hu, F., Liu, H., 2004. Using a Modified Soil-Plant-Atmosphere Scheme (MSPAS) to Simulate the Interaction between Land Surface Processes and Atmospheric Boundary Layer in Semi-Arid Regions. Adv. Atmos. Sci. 21 (2), 15. https://doi.org/10.1007/BF02915711.

...Liu, S.M., Li, X., Xu, Z.W., Che, T., Xiao, Q., Ma, M.G., Wang, W.Z., 2018b. The Heihe Integrated Observatory Network: a basinscale land surface processes observatory in China. Vadose Zone J. 17 (1). https://doi.org/10.2136/vzj2018.04.0072.

Liu, S.M., Xu, Z.W., Song, L.S., Zhao, Q.Y., Ge, Y., Xu, T.R., Zhang, F., 2016. Upscaling evapotranspiration measurements from multi-site to the satellite pixel scale over heterogeneous land surfaces. Agric. For. Meteorol. 230, 97–113. https://doi.org/10.1016/j.agrformet.2016.04.008.

Liu, S.M., Xu, Z.W., Wang, W.Z., Bai, J., Jia, Z.Z., Zhu, M.J., Wang, J.M., 2011. A comparison of eddy-covariance and large aperture scintillometer measurements with respect to the energy balance closure problem. Hydrol. Earth Syst. Sci. 15 (4), 1291–1306. https://doi.org/10.5194/hess-15-1291-2011.

Ma, Y.F., Liu, S.M., Song, L.S., Xu, Z.W., Liu, Y.L., Xu, T.R., Zhu, Z.L., 2018. Estimation of daily evapotranspiration and irrigation water efficiency at a Landsat-like scale for an arid irrigation area using multi-source remote sensing data. Remote Sens. Environ. 216, 715–734. https://doi.org/10.1016/j.rse.2018.07.019.

Macqueen, J.T., Draxler, P.R., Rolph, G.D., 1995. Influence of grid size and terrain resolution on wind field predictions from an operational mesoscale model. J. Appl. Meteorol. 34 (10), 2166–2181 10.1175/1520-0450(1995)034<2166:IOGSAT>2.0.CO;2.

Manickathan, L., Defraeye, T., Allegrini, J., Derome, D., Carmeliet, J., 2018. Parametric study of the influence of environmental factors and tree properties on the transpirative cooling effect of trees. Agric. For. Meteorol. 248, 259–274. https://doi.org/10.1016/j.agrformet.2017.10.014.

Meng, X., Lü, S., Gao, Y., Guo, J., 2015. Simulated effects of soil moisture on oasis self-maintenance in a surrounding desert environment in Northwest China. Int. J. Climatol. 35 (14), 4116–4125. https://doi.org/10.1002/joc.4271.

Meng, X., Lü, S., Zhang, T., Ao, Y., Li, S., Bao, Y., Wen, L., Luo, S, 2012. Impacts of inhomogeneous landscapes in oasis interior on the oasis self-maintenance mechanism by integrating numerical model with satellite data. Hydrol. Earth Syst. Sci. 16 (10), 3729–3738. https://doi.org/10.5194/hess-16-3729-2012.

...Meng, X., Lü, S., Zhang, T., Guo, J., Gao, Y., Bao, Y., Liu, Y., 2009. Numerical simulations of the atmospheric and land conditions over the jinta oasis in northwestern china with satellite-derived land surface parameters. J. Geophys. Res. Atmos. 114 (D6), 605–617. https://doi.org/10.1029/2008JD010360.

Oke, T.R., Cleugh, H.A., 1987. Urban heat storage derived as energy balance residuals. Boundary Layer Meteorol. 39 (3), 233–245. https://doi.org/10.1007/BF00116120.

Patankar, S.V., 1981. A calculation procedure for two-dimensional elliptic situations. Numer. Heat Transf. 4 (4), 409–425. https://doi.org/10.1080/01495728108961801.
Patton, E.G., Sullivan, P.P., Moeng, C.H., 2005. The influence of idealized heterogeneity on wet and dry planetary boundary layers coupled to the land surface. J. Atmos. Sci. 62 (7), 2078–2097. https://doi.org/10.1175/JAS3465.1.
PielkeSr, R.A., 2001. Influence of the spatial distribution of vegetation and soils on the prediction of cumulus convective rainfall. Rev. Geophys. 39 (2), 151–177. https://doi.org/10.1029/1999RG000072.
Pieterse, J.E., Harms, T.M., 2013. CFD investigation of the atmospheric boundary layer under different thermal stability conditions. J. Wind Eng. Indust. Aerodyn. 121, 82–97. https://doi.org/10.1016/j.jweia.2013.07.014.
Potchter, O., Goldman, D., Kadish, D., Iluz, D., 2008. The oasis effect in an extremely hot and arid climate: the case of southern Israel. J. Arid Environ. 72 (9), 1721–1733. https://doi.org/10.1016/j.jaridenv.2008.03.004.
Richards, P.J., Hoxey, R.P., 1993. Appropriate boundary conditions for computational wind engineering models using the k-ε turbulence model. J. Wind Eng. Indust. Aerodyn. 46, 145–153. https://doi.org/10.1016/0167-6105(93)90124-7.
Saaroni, H., Bitan, A., Dor, E.B., Feller, N., 2004. The mixed results concerning the 'oasis effect' in a rural settlement in the Negev Desert, Israel. J. Arid Environ. 58 (2), 235–248. https://doi.org/10.1016/j.jaridenv.2003.08.010.
Scanlon, B.R., Keese, K.E., Flint, A.L., Flint, L.E., Gaye, C.B., Edmunds, W.M., Simmers, I., 2006. Global synthesis of groundwater recharge in semiarid and arid regions. Hydrol. Process. 20 (15), 3335–3370. https://doi.org/10.1002/hyp.6335.
Sogachev, A., 2009. A note on two-equation closure modelling of canopy flow. Boundary Layer Meteorol. 130 (3), 423–435. https://doi.org/10.1007/s10546-008-9346-2.
Sogachev, A., Kelly, M., Leclerc, M.Y., 2012. Consistent Two-Equation Closure Modelling for Atmospheric Research: buoyancy and Vegetation Implementations. Boundary Layer Meteorol. 145 (2), 307–327. https://doi.org/10.1007/s10546-012-9726-5.
Sogachev, A., Leclerc, M.Y., Karipot, A., Zhang, G., Vesala, T., 2005. Effect of clearcuts on footprints and flux measurements above a forest canopy. Agric. For. Meteorol. 133 (1–4), 182–196. https://doi.org/10.1016/j.agrformet.2005.09.008.
Sogachev, A., Menzhulin, G.V., Heimann, M., Lloyd, J., 2002. A simple three-dimensional canopy - planetary boundary layer simulation model for scalar concentrations and fluxes. Tellus 54B, 784–819. https://doi.org/10.1034/j.1600-0889.2002.201353.x.
Stanev, E., Staneva, J., Bullister, J., Murray, J., 2004. Ventilation of the Black Sea pycnocline. Parameterization of convection, numerical simulations and validations against observed chlorofluorocarbon data. Deep Sea Res. Part I Oceanograph. Res. Papers 51 (12), 2137–2169. https://doi.org/10.1016/j.dsr.2004.07.018.
Stone, K.B., 2015. Burke-Litwin Organizational Assessment Survey: reliability and Validity. Org. Dev. J. 33 (2).
Su, C.X., Hu, Y.Q., 1988. Structure of the planetary boundary layer over oasis cold island. J. Meteorol. Res. 2 (4), 527–534.
Taha, H., Akbari, H., Rosenfeld, A., 1991. Heat island and oasis effects of vegetative canopies: micro-meteorological field-measurements. Theor. Appl. Climatol. 44 (2), 123–138. https://doi.org/10.1007/BF00867999.
Tominaga, Y., Stathopoulos, T., 2007. Turbulent Schmidt numbers for CFD analysis with various types of flowfield. Atmos. Environ. 41 (37), 8091–8099. https://doi.org/10.1016/j.atmosenv.2007.06.054.
...Wang, L., Lee, X., Schultz, N., Chen, S., Wei, Z., Fu, C., Lin, G., 2018. Response of surface temperature to afforestation in the Kubuqi Desert, Inner Mongolia. J. Geophys. Res. 123 (2), 948–964. https://doi.org/10.1002/2017JD027522.
Wang, X., Chen, F., Hasi, E., Li, J., 2008. Desertification in China: an assessment. Earth-Sci. Rev. 88 (3–4), 188–206.
Wang, X., Li, Y., 2016. Predicting urban heat island circulation using CFD. Building Environ. 99, 82–97. https://doi.org/10.1016/j.buildenv.2016.01.020.
Wang, X., Li, Y., Wang, K., Yang, X., Chan, P.W., 2017. A simple daily cycle temperature boundary condition for ground surfaces in CFD predictions of urban wind flows. J. Appl. Meteorol. Climatol. 56 (11), 2963–2980. https://doi.org/10.1175/JAMC-D-17-0095.1.
Weiss, M., Baret, F., Smith, G.J., Jonckheere, I., Coppin, P., 2004. Review of methods for in situ leaf area index (LAI) determination: part II. Estimation of LAI, errors and sampling. Agric. For. Meteorol. 121 (1–2), 37–53. https://doi.org/10.1016/j.agrformet.2003.08.001.
Wen, X., Liao, X., Yuan, W., Yan, X., Wei, Z., Liu, H., Feng, J., Lu, S., Dong, W., 2014. Numerical simulation and data assimilation of the water-energy cycle over semiarid northeastern China. Sci. China Earth Sci. 57 (10), 2340–2356. https://doi.org/10.1007/s11430-014-4914-4.
Wu, L., Chao, J., Fu, C., Pan, X, 2003. On a Simple Dynamics Model of Interaction between Oasis and Climate. Adv. Atmos. Sci. 20 (5), 6.
...Xu, T., Guo, Z., Liu, S., He, X., Meng, Y., Xu, Z., Song, L., 2018. Evaluating different machine learning methods for upscaling evapotranspiration from flux towers to the regional scale. J. Geophys. Res. 123 (16), 8674–8690. https://doi.org/10.1029/2018JD028447.
...Xu, T., He, X., Bateni, S.M., Auligne, T., Liu, S., Xu, Z., Mao, K., 2019. Mapping regional turbulent heat fluxes via variational assimilation of land surface temperature data from polar orbiting satellites. Remote Sens. Environ. 221, 444–461. https://doi.org/10.1016/j.rse.2018.11.023.
Xu, Z.W., Ma, Y.F., Liu, S.M., Shi, W.J., Wang, J.M., 2017. Assessment of the Energy Balance Closure under Advective Conditions and Its Impact Using Remote Sensing Data. J. Appl. Meteorol. Climatol. 56 (1), 127–140. https://doi.org/10.1175/JAMC-D-16-0096.1.
..Xue, J., Gui, D., Lei, J., Sun, H., Zeng, F., Mao, D., Liu, Y., 2018. Oasis microclimate effects under different weather events in arid or hyper arid regions: a case analysis in southern Taklimakan desert and implication for maintaining oasis sustainability. Theor. Appl. Climatol. 1–13. https://doi.org/10.1007/s00704-018-2567-5.
Yamada, T., 1982. A numerical model study of turbulent airflow in and above a forest canopy. J. Meteorol. Soc. Jpn. Ser. II 60 (1), 439–454. https://doi.org/10.2151/jmsj1965.60.1_439.
Yamada, Y., Kirillova, I., Peschon, J.J., Fausto, N., 1997. Initiation of liver growth by tumor necrosis factor: deficient liver regeneration in mice lacking type I tumor necrosis factor receptor. Proc. Natl. Acad. Sci. 94 (4), 1441–1446. https://doi.org/10.1073/pnas.94.4.1441.
Zhang, K., An, Z., Cai, D., Guo, Z., Xiao, J., 2017. Key Role of Desert-Oasis Transitional Area in Avoiding Oasis Land Degradation from Aeolian Desertification in Dunhuang, Northwest China. Land Degrad. Dev. 28 (1), 142–150. https://doi.org/10.1002/ldr.2584.
Zhang, N., Wang, X., Peng, Z., 2014. Large-eddy simulation of mesoscale circulations forced by inhomogeneous urban heat island. Boundary Layer Meteorol. 151 (1), 179–194. https://doi.org/10.1007/s10546-013-9879-x.
Zhang, Q., Hu, Y.J., Zhao, M., 1998. PBL characteristic simulation under desert-oasis interaction. J. Nanjing Inst. Meteorol. 21 (1), 104–113 (In Chinese).
Zhang, Q., Huang, R., 2004. Water vapor exchange between soil and atmosphere over a Gobi surface near an oasis in the summer. J. Appl. Meteorol. 43 (12), 1917–1928 (In Chinese).
Zhang, Q., Yu, X.Q., 2001. Numerical simulation of oasis-induced mesoscale atmospheric flow and its sensitivity test of key factors. Plateau Meteorol. 20 (1), 58–65 (In Chinese).
Zhao, R., Chen, Y., Shi, P., Zhang, L., Pan, J., Zhao, H., 2013. Land use and land cover change and driving mechanism in the arid inland river basin: a case study of Tarim River, Xinjiang, China. Environ. Earth Sci. 68 (2), 591–604. https://doi.org/10.1007/s12665-012-1763-3.
Zhao, W., Hu, G., Zhang, Z., He, Z., 2008. Shielding effect of oasis-protection systems composed of various forms of wind break on sand fixation in an arid region: a case study in the Hexi Corridor, northwest China. Ecol. Eng. 33 (2), 119–125. https://doi.org/10.1016/j.ecoleng.2008.02.010.
Zhou, Y., Li, D., Liu, H., Li, X., 2018. Diurnal variations of the flux imbalance over homogeneous and heterogeneous landscapes. Boundary Layer Meteorol. 168 (3), 417–442. https://doi.org/10.1007/s10546-018-0358-2.
Zhu, X., Ni, G., Cong, Z., Sun, T., Li, D., 2016. Impacts of surface heterogeneity on dry planetary boundary layers in an urban-rural setting. J. Geophys. Res. 121 (20), 12–164. https://doi.org/10.1002/2016JD024982.